Late Cretaceous Transtension in the Eastern Tibetan Plateau: Evidence from Postcollisional A-type Granite and Syenite in the Changdu area, China

Xin-Song Wang [1, 2], A.E. Williams-Jones [2], Xian-Wu Bi [1], Rui-Zhong Hu [1], Jia-Fei Xiao [1], and Ming-Liang Huang [1, 3]

[1]State Key Laboratory of Ore Deposit Geochemistry, Institute of Geochemistry, Chinese Academy of Sciences, Guiyang 550081, China

[2]Department of Earth and Planetary Sciences, McGill University, 3450 University Street, Montréal, Québec, Canada H3A 2A7

[3]University of Chinese Academy of Sciences, Beijing 100049, China

Corresponding author: Xian-Wu Bi (bixianwu@vip.gyig.ac.cn)

Key Points:

- The Bangda A-type granite and Ruduo syenite were emplaced along the Longmu-Shuanghu Suture zone at ~78 Ma and ~74 Ma, respectively.
- The two intrusions were derived from partial melting of alkali-rich basaltic lower crust with a minor contribution of mantle melt.
- Late Cretaceous transtension followed the Lhasa-Qiangtang collision in the Eastern Tibetan Plateau.

Wang, X.-S., Williams-Jones, A.E., Bi, X.-W., Hu, R.-Z., Xiao, J.-F., & Huang, M.-L. (2019).
J. Geophys. Res., Solid Earth 124, 6409–6427.

Abstract

The Late Cretaceous is an important geological time interval for the Tibetan Plateau because it corresponds to the period when the tectonic regime changed from Lhasa-Qiangtang collision to Indo-Asian assembly. However, the nature of and controls on the change in tectonic regime are poorly constrained. In this paper, we report results of a study of two intrusions in the Changdu area of the Eastern Tibetan Plateau. Zircon U-Pb dating shows that both intrusions formed at ca. 77.6~74.3 Ma. The Bangda intrusion has A-type granite affinity and a peraluminous character, whereas the Ruduo intrusion is a metaluminous syenite. Both intrusions have very similar trace element compositions, slightly enriched zircon $\varepsilon_{Hf}(t)$ values (-9.3 and -1.7), and EM-2-like Sr-Nd-Pb isotope ratios. These features of the two intrusions indicate that their magmas were derived from partial melting of an alkali-rich basaltic lower crust and a small proportion of mantle melt. The occurrence of alkaline intrusions is consistent with Late Cretaceous extension in the Eastern Tibetan Plateau. Based on the results of this study and previous data, we propose an intra-plate extensional tectonic model, in which there was NS-NNW directed Late Cretaceous transtension in the Eastern Tibetan Plateau following the Lhasa-Qiangtang collision. This extension is interpreted to have been triggered by the Bangong-Nujiang slab break-off at around 110 Ma and driven by the far-field subduction of the Neo-Tethys oceanic crust.

1 Introduction

In the past two decades, stratigraphic, petrological, and geochronological evidence have accumulated, which indicate that the assembly of the Lhasa and Qiangtang Terranes caused significant Late Mesozoic crustal thickening, and formation of the Tibetan Plateau prior to the Indo-Asian collision (e.g., Murphy et al., 1997; Yin & Harrison, 2000; Kapp et al., 2003; Kapp et al., 2007; Wilson & Fowler, 2011; Tian et al., 2014; Volkmer et al., 2014; Wang et al., 2014b; Zhao et al., 2017). This has prompted researchers to re-evaluate the contribution of the Indo-Asian collision to the development of the Tibetan Plateau. However, the nature and effects of the Lhasa and Qiangtang assembly are still hotly debated. Kapp et al. (2005) proposed a hard collision model, in which the Lhasa terrane was underthrust northward beneath the Qiangtang terrane during the Early to Mid-Cretaceous, due to flat-slab subduction of Neotethyan oceanic lithosphere along the Indus-Yarlung Zangbo Suture Zone (IYZSZ). Zhang et al. (2012) concluded that northward subduction of the Bangong-Nujiang Meso-Tethyan Oceanic crust beneath the Qiangtang Terrane continued until the two terranes collided in the Late Cretaceous. In contrast to these hypotheses, Zhu et al. (2016) proposed a divergent double subduction model and claimed that the Lhasa-Qiangtang collision was a soft collision that began during the Early Cretaceous (140~130 Ma) and was followed by the Bangong-Nujiang slab break-off and its sinking during the late Early Cretaceous (120~110 Ma). The models referred to above were developed based mainly on geological evidence from the western and central part (~80^{o}–94^{o} E) (Kapp et al., 2005; Zhang et al., 2012; Zhu et al., 2016) and did not consider the eastern part of the Tibetan Plateau (~95^{o} −105^{o} E), which includes the eastern portion of the Lhasa and Qiangtang Terranes, the Yidun Arc, and the Songpan-Ganzi Fold Belt. In addition, the models do not satisfactorily address the issue of the change in the geodynamic regime from Lhasa-Qiangtang collision to Indo-Asia assembly, the nature and controls of which remain a puzzle.

A Cretaceous regional uplift of the Eastern Tibetan Plateau is recorded by Cretaceous apatite fission-track (AFT) and zircon (U-Th)/He ages of the Triassic intrusions in the Qiangtang, Yidun, and Songpan-Ganzi Terranes (Figures 1 and 2; e.g., Lai et al., 2007; Wilson

Wang, X.-S., Williams-Jones, A.E., Bi, X.-W., Hu, R.-Z., Xiao, J.-F., & Huang, M.-L. (2019).
J. Geophys. Res., Solid Earth 124, 6409–6427.

& Fowler, 2011; Tian et al., 2014; Zhao et al., 2017; Leng et al., 2018). This regional uplift, and a suite of Cretaceous A-type and adakite-like intrusions (105 ~ 75 Ma) along the north-south striking Yidun Arc (Figure 1), are variously interpreted to have resulted from collision of the Yidun and Songpan-Ganzi Terranes (Hou et al., 2003), subduction of the Neo-Tethys oceanic crust (Reid et al., 2007) and strike-slip pull-apart extension in a late- or post-collisional environment related to the Lhasa-Qiangtang collision (Wang et al., 2014a; Wang et al., 2014b; Yang et al., 2016). The main problem in satisfactorily interpreting geological events in the Eastern Tibetan Plateau is that the nature of and controls on the relative motion of the Lhasa and Qiangtang terranes and the Yidun Arc have not been well-constrained. However, the poorly studied Late Cretaceous magmatism of the eastern part of the Qiangtang terrane (between the Lhasa Terrane and Yidun Arc), which included the emplacement of metaluminous to peraluminous A-type granites and syenites, helps shed light on this problem.

A-type granites and syenites are widely accepted to reflect lithospheric extension (e.g., Whalen et al., 1987; Maniar & Piccoli, 1989; Eby, 1992; Bonin, 2007; Frost & Frost, 2011), however, the genesis of the two kinds of igneous rocks are still controversial. They are typically alkaline to peralkaline in composition and are considered to be the products of fractional crystallization from mantle-derived magmas with a crustal component (e.g., Eby et al., 1998; Bonin, 2007; Frost & Frost, 2011; Laporte et al., 2014; Litvinovsky et al., 2015; Siegel et al., 2018). A small proportion of A-type granites, however, is metaluminous and peraluminous and interpreted to be derived from partial melting of quartzo-feldspathic meta-igneous or metasedimentary rocks within the middle crust or lower crust (e.g., Whalen et al., 1987; Patiño Douce, 1997; Dall'Agnol & de Oliveira, 2007; Thomsen & Schmidt, 2008; Frost & Frost, 2011; Dai et al., 2017). Some metaluminous and peraluminous A-type-granites, as well as some metaluminous syenites, are interpreted to have been derived from partial melting of a lower crust composed of alkali basalt (e.g., Kaszuba & Wendlandt, 2000; Legendre et al., 2005; Litvinovsky et al., 2015).

The current study is based on two representative acidic intrusions formed in the Late Cretaceous that were recently described in the Changdu area of the Qiangtang Terrane, Eastern Tibetan Plateau. Here, we report on the nature, age and origin of these intrusions, and use the information to contribute new understanding of the Lhasa-Qiangtang collision. A combination of whole-rock geochemistry, Hf-O and Sr-Nd-Pb isotope geochemistry and zircon U-Pb age determinations are used to constrain the petrogenesis and timing of the intrusions. From this information, we make the case that the intrusions were emplaced during Late Cretaceous transtension related to the Lhasa-Qiangtang collision after the Meso-Tethyan slab had broken off, and that this was probably due to the far-field effect of the northward subduction of the Neo-Tethys oceanic crust.

2 Regional geology

The Eastern Tibetan Plateau is a complex assemblage of terranes, which broke off the Gondwanan or Cathaysian paleo-continent. Detrital zircon ages suggest that the Lhasa Terrane separated from Western Australia and the Western Qiangtang Terrane from the Indian plate, both of which were part of Gondwana (Zhu et al., 2011a). The Eastern Qiangtang, Yidun Arc (Zhongza Massif), and Songpan-Ganzi Terranes have a similar basement to the Yangtze Terrane, which is thought to be part of the Cathaysian paleo-continent (Wang et al., 2013a).

2.1 Closure of the Paleo-Tethyan Oceans during the Triassic

The terranes in the Eastern Tibetan Plateau are separated by several Paleo-Tethyan suture zones, namely the Longmu-Shuanghu Suture Zone (LSSZ), the Jinshajiang Suture Zone (JSSZ), and the Ganzi-Litang Suture Zone (GLSZ). From west to east, these suture zones separate the Western Qiangtang, Eastern Qiangtang, Yidun Arc, and Songpan-Ganzi Terranes, respectively (Figures 1a and 1b). Three large arc-type, post-collisional magmatic belts formed along these three suture zones as a result of the closure of the Longmu-Shuanghu, Jinshajiang, and Ganzi-Litang Paleo-Tethyan Oceans, and the assembly of the terranes during the Late Permian and Triassic (e.g., Yin & Harrison, 2000; Zhu et al., 2011a; Yang et al., 2014; Peng et al., 2015). Triassic volcano-sedimentary successions are widely distributed in the Eastern Tibetan Plateau and consist of flysch and volcanic flows (Yang et al., 2014).

Triassic eclogites are exposed along the LSSZ in the Dingqing-Leiwuqi-Basu area of the Eastern Tibetan Plateau (Zhang & Tang, 2009), which is thought to be the eastward extension of the high-pressure to ultra-high-pressure Triassic metamorphic belt that occurs along the LSSZ in the central Tibetan Plateau (Zhang & Tang, 2009; Pullen & Kapp, 2014). A wide back-arc basin and large area of volcanic rocks occur in a 500 km north-south zone that follows the strike of the Yidun Arc. Emplacement of these rocks was triggered by the roll-back of the westward dipping Ganzi-Litang oceanic slab beneath the Zhongza Massif during the Middle and Late Triassic. Bimodal volcanic rocks were generated in the Changtai-Daocheng area in the northern Yidun Arc during the Middle Triassic (~230 Ma; Wang et al., 2013b), indicating that the Arc was in a phase of extension at this time.

2.2 Jurassic and Cretaceous geological records in the Eastern Tibetan Plateau

2.2.1 Basu-Chayu area of the Lhasa Terrane

The Lhasa Terrane is located between the Himalaya and Qiangtang Terranes, and is bounded to the north by the Meso-Tethyan Bangong-Nujiang Suture Zone (BNSZ) and to the south by the Neo-Tethyan Indus-Yarlung Zangbo Suture Zone (IYZSZ) (Figures 1a and 1b). Paleomagnetic data suggest that the Lhasa Terrane was at the same paleolatitude as the Indian Plate at ~240 Ma and has been moving northward since then, reaching the same paleolatitude as the Qiangtang Terrane at ca. ~135 Ma (Song et al., 2017; Figure 2a).

The Jurassic rocks in the region comprise Middle Jurassic limestone, red conglomerate, and sandstone, and Upper Jurassic sandstone and black shale, which are separated from the underlying Triassic strata by an angular unconformity. The overlying rocks comprise Lower Cretaceous sandstone, shale, and andesitic volcanics, which lie beneath a Paleogene molasse and red beds (Table S1).

Four episodes of felsic igneous activity have been recognized in the Basu-Chayu area with ages of ~195 Ma, ~153 Ma, 133~110 Ma, and 66~57 Ma (Chiu et al., 2009). Several studies have suggested that the granitoids representing the two earliest episodes (~195 and ~153 Ma) are genetically related to Jurassic granitoids in the Northern Plutonic belt of central Tibet (Figure 1b). The latter are interpreted by some researchers to have formed during flat subduction of the Neo-Tethyan Indus-Yarlung Zangbo Oceanic lithosphere (Chiu et al., 2009) and by others to record the southward subduction of the Bangong-Nujiang Oceanic slab (Zhu et al., 2011b). There is a similar debate over the genesis of the Early Cretaceous granitoids (133~110 Ma). Either they were products of flat northward subduction of the Neo-Tethyan Oceanic crust (Chiu et al., 2009)

Wang, X.-S., Williams-Jones, A.E., Bi, X.-W., Hu, R.-Z., Xiao, J.-F., & Huang, M.-L. (2019).
J. Geophys. Res., Solid Earth 124, 6409–6427.

or the southward subduction of the Meso-Tethyan Oceanic crust and subsequent slab break-off (Zhu et al., 2011b). The 66~57 Ma granitoids are thought to be genetically related to Neo-Tethyan Oceanic slab roll-back (Chung et al., 2005; Chiu et al., 2009).

2.2.2 The Changdu area of the Qiangtang Terrane

The Jurassic sedimentary rocks of the Changdu area consist of Lower Jurassic red sandstone and siltstone, Middle Jurassic red sandstone and siltstone intercalated with bioclastic limestone, and Upper Jurassic red sandstone, siltstone, and mudstone. The Cretaceous rocks comprise red sandstone and conglomerate, which are separated from the Jurassic sedimentary rocks by an angular unconformity (Table S1).

According to regional geological survey reports, the Jurassic and Early Cretaceous magmatism is poorly represented in the Changdu area. Several Late Cretaceous syenites and A-type granitic intrusions (77.6~74.3 Ma; this study) are exposed in the Leiwuqi-Zuogong part of this area along the LSSZ (Figures 1b-1d). There are also Cenozoic alkaline intrusions (~40 Ma), which were emplaced along strike-slip faults thought to have been triggered by the Indo-Asian collision (Chung et al., 2005).

2.2.3 The Yidun Arc and Songpan-Ganzi Terrane

In the Yidun Arc, Paleogene molasse and red beds unconformably overlie Triassic flysch, calcareous rocks and calc-alkaline rhyolitic volcanics. Jurassic and Cretaceous strata were rarely deposited in the Yidun Arc and only a few Jurassic nonmarine strata and intrusions are observed (Reid et al., 2007; Wang at al., 2014b; Jackson et al., 2018; Table S1). The latter are thought to represent postcollisional magmas related to collision of the Yidun and Songpan-Ganzi Terranes (Qu et al., 2003; Wu et al., 2014). In contrast, during the Cretaceous, large volumes of intrusive rocks were emplaced along north-south striking faults in the Yidun Arc, i.e., the Dege-Xiangcheng-Geza faults (DXGF). In the northern Yidun Arc, the intrusions are dominantly A-type granites with ages ranging from 105 Ma to 75 Ma. These intrusions have high SiO_2 (72.3~76.3 wt.%) and Zr+Nb+Ce+Y (270~442 ppm) contents, a Ga/Al ratio of 2.49~4.24, a zircon εHf value of −3.9 to 0.0, whole-rock εNd values of −8.40 to −4.96 and variable initial $^{87}Sr/^{86}Sr$ ratios (0.7032 to 0.7220) (Qu et al., 2002; Reid et al., 2007). According to Qu et al. (2002), these intrusions resulted from the mixing of metasediment-derived melts with small proportions of mantle-derived melts. In the southern Yidun Arc, the intrusions have adakite-like compositions with variable SiO_2 contents (65~70 wt.%), variable Sr/Y (22–72), and La/Yb (37–69) ratios, zircon εHf values of −7.9 to −2.3, $\delta^{18}O$ values ranging from 5.9 ‰ to 8.4‰, whole-rock εNd values of −8.5 to −5.3 and initial $^{87}Sr/^{86}Sr$ ratios of 0.7069 to 0.7098 (Wang et al., 2014a; Wang et al., 2014b; Yang et al., 2016). Their ages vary from 87 to 76 Ma (Wang et al., 2014a). Wang et al. (2014b) concluded that these intrusions were derived mainly from partial melting of a thickened lower crust and to a minor extent the mantle.

The Songpan-Ganzi Terrane is covered by a Triassic flysch that was initially 10-15 km thick (Table S1). The flysch was strongly folded during the Late Triassic closure of the Paleo-Tethyan Ocean and subsequent collision between the Songpan-Ganzi Terrane and the Yidun Arc. Two generations of granitoids, namely synorogenic granites (220~190 Ma) and postorgenic granites (188~153 Ma) are exposed in the terrane (Tian et al., 2014).

Wang, X.-S., Williams-Jones, A.E., Bi, X.-W., Hu, R.-Z., Xiao, J.-F., & Huang, M.-L. (2019).
J. Geophys. Res., Solid Earth 124, 6409–6427.

2.3 The intrusions of this study

The Ruduo (Figure 1c) and Bangda (Figure 1d) intrusions investigated in this study are located in the Western Qiangtang Terrane, along the LSSZ (Figure 1b). The Bangda intrusion is about 70 km southeast of the Ruduo intrusion (N 30° 40' 10.03", E 97° 08' 22.98") and is exposed over an area of ~ 6000 m^2. It is a biotite granite porphyry composed of 25–35 vol.% K-feldspar, 30–40 vol.% plagioclase, 25–30 vol.% quartz, and 5–10 vol.% biotite (Figures 3a-3c). Accessory minerals include zircon, apatite, and titanite. The Ruduo intrusion is a small stock exposed in Ruduo village (N 31° 06' 43.07", E 96° 41' 57.32") and intruded Permian gneissic granites (Figure 1c). It is a syenite containing 35–45 vol.% K-feldspar, 45–50% vol.% albite, 1–5 vol.% muscovite and 1–5 vol.% carbonate minerals (Figures 3d-3h). The main accessory minerals are zircon, monazite, apatite, and pyrite. Samples from the two intrusions were collected along a traverse corresponding to the long axis of the intrusions.

3 Results

Details of the analytical methods and formulae are given in Text S1 and Tables S2–S7 in the supporting information (Keto and Jacobsen, 1987; Wiedenbeck et al., 1995; Todt et al., 1996; Blichert-Toft and Albarède, 1997; Qi et al., 2000; Tanaka et al., 2000; Griffin et al., 2000; Scherer et al., 2001; Griffin et al., 2002; Ludwig, 2003; Zhang et al., 2006; Liu et al., 2010; Li et al., 2013; Li et al., 2015; Liu et al., 2017). Results of laser ablation inductively coupled plasma mass spectrometric (LA-ICP-MS), zircon U-Pb isotopic (geochronological), zircon Hf-O isotopic, whole-rock major and trace element, and Sr-Nd-Pb isotopic analyses for the samples are given in Tables S2–S7.

3.1 Zircon U-Pb age

The ages of the Ruduo and Bangda intrusions were determined using zircon crystals extracted from samples RD15-01 and BD15-07, respectively (Table S2). The zircon crystals from these samples are euhedral, colorless, and display oscillatory zoning in CL images. No inherited cores were observed in the crystals from sample BD15-07 but several crystals with inherited cores were extracted from sample RD15-01 (Figure 4c).

Twenty-seven analyses were conducted on twenty-two zircon crystals from sample RD15-01 (Table S2). Three crystals with inherited cores yielded Paleoproterozoic ages (analytical points 24, 25, 33, 34, and 13). The $^{206}Pb/^{238}U$ model ages for these cores range from 1022 to 1670 Ma, the $^{207}Pb/^{235}U$ model ages are from 1295 to 1749 Ma, and the $^{207}Pb/^{206}Pb$ model ages from 1391 to 1780 Ma (Figure 4c). A further eight analyses of inherited cores yielded $^{206}Pb/^{238}U$ model ages varying from 87.8 to 83.8 Ma and $^{207}Pb/^{235}U$ model ages ranging from 89.9 to 81.1 Ma (analytical points 4, 6, 12, 17, 26, 29, 32, and 35). The weighted mean age was 85.5 ± 1.2 Ma (2σ, MSWD = 2.3). The remaining fourteen analytical points, including three points on the outer parts of crystals that had inherited cores, returned $^{206}Pb/^{238}U$ model ages from 77.5 to 73.3 Ma. All the model ages are concordant and the weighted mean $^{206}Pb/^{238}U$ model age is 74.3 ± 0.8 Ma (2σ, MSWD = 3.8) (Figures 4a and 4b). The zircon crystals with the youngest $^{206}Pb/^{238}U$ model ages display growth zones indicating that they crystalized from the magma directly. Their weighted mean age of 74.3 ± 0.8 Ma is interpreted to be the age of the Ruduo intrusion.

Seventeen analyses of zircon crystals from sample BD15-07 yielded $^{206}Pb/^{238}U$ model ages of 81.4 Ma to 73.8 Ma and $^{207}Pb/^{235}U$ model ages of 83.5 to 75.0 Ma (Table S2). All the

Wang, X.-S., Williams-Jones, A.E., Bi, X.-W., Hu, R.-Z., Xiao, J.-F., & Huang, M.-L. (2019).
J. Geophys. Res., Solid Earth 124, 6409–6427.

model ages are concordant and the weighted mean $^{206}Pb/^{238}U$ model age is 77.6 ± 0.9 Ma (2σ, MSWD = 5.6) (Figure 4d), which is interpreted to be the age of the Bangda intrusion.

3.2 Zircon O isotope ratios

Twenty-six oxygen isotopic analyses were conducted on zircon crystals from the Ruduo syenite prior to U-Pb dating (Tables S2 and S3). The $\delta^{18}O$ values of the cores of zircon crystals with Paleoproterozoic ages ranged from 5.9 ‰ to 11.3 ‰. In contrast, the range of $\delta^{18}O$ values for cores (inherited) of zircon crystals with ages ranging from 87.8 to 83.8 Ma is narrower and overall higher, i.e., from 9.2 ‰ to 12.3 ‰ (Figure 4c; Table S2). The $\delta^{18}O$ values of the analytical points yielding $^{206}Pb/^{238}U$ model ages from 77.5 to 73.3 Ma vary from 7.8 ‰ to 10.2 ‰, and the weight mean value is 9.3 ± 0.3‰ (2σ) (Figure S1). Twenty zircon crystals from the Bangda granite yielded $\delta^{18}O$ values ranging from 8.0‰ to 11.9‰ and a weight mean of 9.8 ± 0.3‰ (2σ) (Figure S1).

3.3 Zircon Hf isotopic ratios

Values of $\varepsilon_{Hf}(t)$ and two-stage model ages (T_{DM2}) for sample RD15-01 (Ruduo intrusion) were calculated assuming an age of crystallization of 74.3 Ma (Table S4). Twenty zircon crystals without inherited cores yielded $\varepsilon_{Hf}(t)$ values between -7.9 and -1.7, corresponding to T_{DM2} model ages of 1.64 to 1.25 Ga (Figure S1). The $\varepsilon_{Hf}(t)$ values and T_{DM2} ages of sample BD15-07 were calculated for a crystallization age of 77.6 Ma. Twenty-three zircon crystals yielded $\varepsilon_{Hf}(t)$ values between -9.3 and -4.4 reflecting T_{DM2} ages of 1.71 to 1.42 Ga (Figure S1).

3.4 Major and trace elements

The major and trace element compositions of the Ruduo and Bangda intrusions are listed in Table S5. The Ruduo intrusion has high Na_2O (6.83–7.38 wt.%), K_2O (4.87–5.50 wt.%), Na_2O+K_2O (12.1–12.3 wt.%), Al_2O_3 (18.6–19.0 wt.%), and Zr+Nb+Ce+Y contents (363–409 ppm) contents, and a high Ga/Al ratio (2.42–2.64). The contents of SiO_2 (61.9–63.3 wt.%), CaO (1.32–1.76 wt.%), $Fe_2O_3^T$ (1.02–1.54 wt.%) and MgO (0.38–0.55 wt.%) are relatively low. This composition classifies the Ruduo intrusion as a syenite (Figure 5a). The A/CNK (0.92–0.96), A/NK (1.09–1.11), and $FeO^T/(FeO^T+MgO)$ (0.65–0.73) ratios indicates that it is metaluminous, alkaline, magnesian, and oxidized (Figures 5c and 5d).

The Bangda intrusion is a peraluminous, calc-alkaline, magnesian, and oxidized granite (A/CNK = 1.08–1.10 and A/NK = 1.31–1.39, and $FeO^T/(FeO^T+MgO)$ = 0.77–0.80; Figure 5). The contents of the major element oxides are as follows: SiO_2 (69.6–72.6 wt.%), Na_2O (2.94–3.00 wt.%), K_2O (5.05–5.45 wt.%), and Na_2O+K_2O (8.04–8.39 wt.%). The Ga/Al ratio (2.98–3.11, >2.6) and Zr+Nb+Ce+Y content (309–448, mostly >350 ppm) are high, which is also the case for the Ruduo intrusion. The composition of the Bangda intrusion classifies it as an A-type granite (Figures 5a and 5b). In plots of K_2O versus SiO_2 and K_2O versus Na_2O (Figures 5e and 5f), both the Bangda and Ruduo intrusions show potassic (shoshonitic) affinity, however, both intrusions display low MgO* = $MgO/(MgO + FeO^T)$ values (0.20~0.35).

The chondrite-normalized rare earth element (REE) and primitive mantle-normalized trace element profiles of the Bangda and Ruduo intrusions are remarkably similar. Both intrusions display highly fractionated REE patterns with La/Yb ratios of 16–28 and negative Eu anomalies (Eu/Eu* = 0.34–0.48) (Figure 6a), and both show negative Ba, Nb, Sr, P, and Ti anomalies, and positive Rb and Th anomalies (Figure 6b). The two intrusions have relatively low

Sr (98.3–174 ppm) and Ba (279–467 ppm) contents. The Ruduo intrusion, however, is much more enriched in U than the Bangda intrusion.

3.5 Whole-rock Sr, Nd, and Pb isotope ratios

The Sr and Nd isotope ratios of the Bangda and Ruduo intrusions are reported in Table S6 and the Pb isotope ratios in Table S7. The initial isotopic ratios for the Ruduo and Bangda intrusions were corrected to 74.3 Ma and 77.6 Ma, respectively. The Bangda intrusion (six samples) displays a very narrow range of initial $^{87}Sr/^{86}Sr$ (0.7103–0.7117) ratios. The range of $\varepsilon_{Nd}(t)$ values is also narrow (-7.5 to -8.0) and is reflected in the narrow range of T_{DM2} ages of 1.49–1.53 Ga. The Pb isotope ratios are: $(^{206}Pb/^{204}Pb)_t$ from 18.610 to 18.881; $(^{207}Pb/^{204}Pb)_t$ from 15.686 to15.702 and $(^{208}Pb/^{204}Pb)_t$ from 38.952 to 38.970. The Ruduo intrusion (three samples) has slightly higher initial $^{87}Sr/^{86}Sr$ ratios (0.7170–0.7177) and $\varepsilon_{Nd}(t)$ values (-8.6 to -9.0) than the Bangda intrusion (T_{DM2} = 1.58–1.61 Ga). The Pb isotope ratios are: $(^{206}Pb/^{204}Pb)_t$ from 18.362 to 18.487; $(^{207}Pb/^{204}Pb)_t$ from 15.671 to 15.677 and $(^{208}Pb/^{204}Pb)_t$ from 38.632 to 38.652.

4 Discussion

4.1 Petrogenesis of the Ruduo syenite and Bangda A-type granite

The results of this study show that the Ruduo syenite and Bangda A-type granite have remarkably similar REE and trace element profiles (Figures 6a and 6b), and Sr-Nd-Pb-Hf-O isotopic compositions (Figure 7), suggesting that they were derived from a similar source. As mentioned earlier three hypotheses have been proposed for the genesis of A-type granite and syenite magmas: (1) partial melting of mantle followed by fractional crystallization and assimilation (e.g., Eby et al., 1998; Bonin, 2007; Frost & Frost, 2011; Laporte et al., 2014; Litvinovsky et al., 2015; Siegel et al., 2018) ; (2) partial melting of quartzo-feldspathic meta-igneous or metasedimentary rocks within middle crust or lower crust or the orogenic zones that are under high pressure (e.g., Whalen et al., 1987; Patiño Douce, 1997; Dall'Agnol & de Oliveira, 2007; Thomsen & Schmidt, 2008; Frost & Frost, 2011; Dai et al., 2017); and (3) partial melting of alkali basalts in the lower crust (e.g., Kaszuba & Wendlandt, 2000; Legendre et al., 2005; Litvinovsky et al., 2015).

The EM-2-like Sr-Nd-Pb isotopic compositions of the Bangda and Ruduo intrusions suggest that there was a substantial contribution of an EM-2-like component to their magmas (Figure 7). Although the alkaline and metaluminous Ruduo syenite may have crystallized from a mantle derived melt that underwent fractional crystallization and assimilation (Laporte et al., 2014; Figure 8), this is very unlikely to have been the case for the peraluminous, calc-alkaline, and magnesian Bangda A-type granite (Figures 5c and 5d). The reason for this is that A-type granites generated from mantle-derived melts, even after crustal assimilation, show alkaline/peralkaline and ferroan affinities (Eby et al., 1998; Bonin, 2007; Frost & Frost, 2011; Litvinovsky et al., 2015; Siegel et al., 2018). In addition, mantle-derived potassic felsic or syenitic magmas invariably have high MgO* values (0.47~0.76; e.g., Lu et al., 2013; Condamine and Médard, 2014; Laporte et al., 2014), i.e., much higher than those of the Bangda and Ruduo intrusions (MgO* = 0.20~0.35). The positive correlation of CaO, FeO^T, and MgO (Figure 8) with the silica content of the two intrusions, also make an origin for the magmas via fractional crystallization unlikely.

Compared to rocks representing the regional upper crust in the Changdu Area, i.e., the Amdo orthogneiss (Harris et al., 1988; Figure 7c), however, and S-type granites that are also in the area (Dongdashan) and were derived from Late Triassic metasedimentary rocks [$\varepsilon_{Hf}(t)$ (-18.3 to ~ -8.4) and T_{DM2}^{Hf} model ages (2.41~1.81 Ga)] (Peng et al., 2015; Figures 6b and 6c), the Bangda A-type granite and Ruduo syenite have higher zircon $\varepsilon_{Hf}(t)$ values (-9.3 and -1.7), younger T_{DM2}^{Hf} model ages (1.71~1.25 Ga) and depleted Sr and Nd isotope values (Figure 7). These observations indicate that the two intrusions could not have had an origin similar to that of the Dongdashan granites, which are interpreted to have been derived primarily from partial melting of old metasedimentary rocks (Peng et al., 2015). In addition, there is no evidence to suggest that it is possible to generate syenite magmas through partial melting of quartzo-feldspathic metasedimentary or quartzo-feldspathic meta-igneous rocks. In principle, syenites could be products of high pressure (2.5~5.0 GPa) partial melting of calcareous Fe-bearing rocks (Thomsen & Schmidt, 2008). However, high pressure partial melting models generate magmas with high Sr contents (mostly >160 ppm), and high K_2O/Na_2O (mostly >2; Figure 8) and La/Yb (mostly > 39) ratios (Thomsen & Schmidt, 2008; Dai et al., 2017), whereas the data presented above show that the corresponding values for the Bangda and Ruduo intrusions are much lower.

From the geochemical and isotopic data presented above, it is evident that fractional crystallization of contaminated mantle-derived melts and partial melting of quartzo-feldspathic meta-igneous or metasedimentary rocks cannot satisfactorily explain the genesis of the two intrusions. Instead, it is much more likely that they were the products of partial melting of basaltic lower crust having the isotopic composition of EM-2.

Numerous experimental studies have shown that at high pressure (1.0~3.2 GPa), partial melting of basaltic rocks will generate melts with Sr contents greater than 400 ppm, and high $Sr/Y \geq 20$ and $La/Yb \geq 20$ ratios, i.e., melts of adakitic affinity, because of increases in the proportions of residual pyroxene, and garnet with increasing pressure (e.g., Rapp et al., 1991; Wolf and Wyllie, 1994; Rapp and Watson, 1995; Winther, 1996; Xiao & Clemens, 2007; Qian and Hermann, 2013). However, the Bangda and Ruduo intrusions have similar negative Eu*/Eu values, low Sr (98.3 –174 ppm) and Ba (279 – 467 ppm) contents, and low La/Yb (16 – 28) and Sr/Y (4.4 – 7.6) ratios. This is indicative of partial melting in a lower crust of normal thickness (20~30 km), in which plagioclase is a dominant mineral (Stern, 2002). Indeed, partial melting experiments conducted on low K basaltic rocks (e.g., tholeiites, and amphibolite) commonly generate low to moderately potassic or sodic magmas (Figure 5e; e.g., Rapp et al., 1991; Wolf and Wyllie, 1994; Rapp and Watson, 1995; Winther, 1996; Xiao & Clemens, 2007; Qian and Hermann, 2013), whereas partial melting of high K basaltic rocks (e.g., alkali basalts, hornblende-biotite gabbro, and shoshonite) produce shoshonitic or syenitic magmas (Figure 5e; e.g., Rapp and Watson, 1995; Kaszuba & Wendlandt, 2000; Sisson et al., 2005; Xiao & Clemens, 2007). The two intrusions considered in this study display shoshonitic affinities (Figures 5e and 5f), which suggests a high K basaltic source. Therefore, it seems reasonable that the Bangda and Ruduo intrusions were derived from a high K basaltic source within the lower crust. Significantly, Sisson et al., (2005) showed experimentally that partial melting (17~22 wt.% melt) of a high potassium basalt (SiO_2 = ~51 wt.%) at 0.7 GPa, high fO_2 (MnO-Mn_3O_4), and 850~900 ^{o}C will generate a magma compositionally very similar to the Bangda granite (Figure 8). Furthermore, the low $FeO^T/(FeO^T+MgO)$ (0.77~0.80, <0.88) ratio of the Bangda granite is indicative of an oxidized source (Dall'Agnol & de Oliveira, 2007). We therefore propose that the Bangda granite was derived from partial (hydration) melting of an oxidized high K basaltic lower

Wang, X.-S., Williams-Jones, A.E., Bi, X.-W., Hu, R.-Z., Xiao, J.-F., & Huang, M.-L. (2019).
J. Geophys. Res., Solid Earth 124, 6409–6427.

crust containing plagioclase, amphibole, biotite, apatite, and titanomagnetite (Sisson et al., 2005). This hypothesis satisfactorily explains the trace element profile of the Bangda granite, which displays moderately negative Eu, Sr, Ba, P, and Ti anomalies.

Although partial melting of a high K basaltic lower crust satisfactorily explains the genesis of the Bangda magma, such a source could not have produced the Ruduo syenite, which is characterized by high Na_2O and Al_2O_3 contents, and relatively low SiO_2, CaO, $Fe_2O_3^T$ and MgO contents (see above). Based on the partial melting experiments (0.7 GPa) of Sisson et al. (2005) that involved a basaltic source rock, a relatively high-degree of partial melting (~31 wt.% melt) would have been needed to generate melts with the silica and alumina content of the Ruduo syenite (SiO_2: 61.9–63.3 wt.% and Al_2O_3:18.6–19.0 wt.%). A high-degree of partial melting, however, would greatly increase the FeO, MgO and CaO contents, and reduce the Na_2O+K_2O content of the magma, which are much higher and lower, respectively, than those observed (Figure 8; Sisson et al., 2005). Xiao and Clemens, (2007) suggested that high pressure (1.5~2.5 GPa) partial melting of shoshonite could generate syenitic melts, but, as discussed above, this is inconsistent with the low Sr/Y and La/Yb ratios of the Ruduo intrusion. Partial melting of a more mafic source (SiO_2 = ~45 wt.%) at slightly higher temperature (~1050 ^oC) and pressure (0.7~1.0 GPa), corresponding to that at the base of the continental crust (20 – 30 km) would increase the Na_2O, K_2O and Al_2O_3 content of the magma (Figure 8; Kaszuba & Wendlandt, 2000; Condamine and Médard, 2014; Laporte et al., 2014).

Interestingly, the results of experiments of Kaszuba and Wendlandt (2000) suggest that dehydration melting of alkali basalts altered by volatiles (H_2O+CO_2) at 1025 ^oC, 0.7 and 1.0 GPa could generate syenitic magmas of the type that formed the Ruduo syenite (Figure 8). In these experiments, trachyandesitic and trachytic melts were in equilibrium with olivine, clinopyroxene, amphibole, phlogopite, titaniferous magnetite, and plagioclase. If this was the case for the source region of the magma that generated the Ruduo syenite, it could explain the low Fe, Mg, and Ca contents and anomalously negative Ba, Ti, Sr, and Eu concentrations of the Ruduo syenite. Significantly, the Ruduo syenite contains about 1~5% carbonate, which indicates that the magma that crystallized the Ruduo syenite was enriched in CO_2. In addition, we note that the Ruduo syenite displays a slightly depleted Hf isotopic composition, younger T_{DM2}^{Hf} model ages, and lower $\delta^{18}O$ values than the Bangda A-type granite (Figure S1; 7a; 7b). This probably indicates that there was a minor contribution to its source from mantle derived melts.

Given their relatively depleted isotopic compositions and their Proterozoic T_{DM2}^{Hf} model ages (1.71~1.25 Ga) and inherited zircon ages (1.78 – 1.39 Ga and ~85 Ma), two types of mafic lower crust are plausible source rocks for the magmas that generated the Bangda and Ruduo intrusions, namely a late Paleo- to Meso-Proterozoic basaltic lower crust, and a newly underplated basaltic lower crust originating from an EM-2-like mantle. On the basis of petrogenetic studies of the igneous rocks in the Western Qiangtang terrane and northwest India, it is possible that a late Paleo- and Meso-Proterozoic (~1.82 Ga to ~1.2 Ga) basaltic lower crust probably developed under the Changdu area during the assembly or breakup of the Columbia supercontinent (Zhu et al., 2011a). However, it is difficult to envisage such a lower crust melting, if the crust was of normal thickness (20~30 km) as the corresponding temperature would only have been 400–500 °C (Stern, 2002). Partial melting of a Proterozoic mafic lower crust needs sufficient heat or additional water. In contrast to a Proterozoic lower crust, a hot newly underplated basaltic lower crust could easily be melted (Huppert and Sparks, 1988). However, we do not preclude the possibility of a Proterozoic mafic lower crust.

Wang, X.-S., Williams-Jones, A.E., Bi, X.-W., Hu, R.-Z., Xiao, J.-F., & Huang, M.-L. (2019).
J. Geophys. Res., Solid Earth 124, 6409–6427.

In short, the Bangda A-type granite and Ruduo syenite were both derived by partial melting of an alkali basaltic lower crust. The crust responsible for generating the Ruduo syenite magma, however, was more mafic and had been altered by the influx of CO_2 and H_2O and with a minor contribution of mantle derived melts. We, therefore, propose a genetic model for the Bangda A-type granite and Ruduo syenite in which, 1) a Late Cretaceous tectonic event triggered partial melting of enriched subcontinental lithospheric mantle and underplating of basaltic magmas and, 2) partial melting of heterogenous alkali lower crust at ca. 77.6~74.3 Ma generated the two intrusions. Given that the genesis of alkaline igneous rocks, including syenite and A-type granite, is facilitated by an extensional tectonic setting (Whalen et al., 1987; Maniar & Piccoli, 1989; Eby, 1992; Bonin, 2007; Frost & Frost, 2011), we further propose that the ca. 77.6~74.3 Ma emplacement of the Bangda and Ruduo intrusions was the result of Late Cretaceous intra-plate extension.

4.2 The assembly of the Lhasa and Qiangtang Terranes in the Eastern Tibetan Plateau

Northward and divergent double subduction models have been proposed to explain the assembly of the Lhasa and Qiangtang Terranes, based on studies of the Central Tibetan Plateau (Kapp et al., 2005; Zhang et al., 2012; Zhu et al., 2016). Jurassic and Early Cretaceous igneous rocks, however, are rarely observed in the Changdu area (location of the Bangda and Ruduo intrusions) of the Qiangtang Terrane and Yidun Arc/Songpan-Ganzi Terrane. On the other hand, they are common in the Basu-Chayu area of the Lhasa Terrane. This differs considerably from the situation in the central Tibetan Plateau, where large volumes of Jurassic and Early Cretaceous subduction-related magmas are distributed on both sides of the Bangong-Nujiang Suture Zone (Zhang et al., 2012; Zhu et al., 2016 and references therein). In addition, the sedimentary rocks in the Changdu area evolved from shallow marine sediments in the Middle Jurassic to red beds and conglomerates in the Cretaceous (Table S1), indicating that the Changdu area evolved from a Jurassic littoral zone to a Cretaceous foreland basin. Flysch and volcano-sedimentary successions of Middle Jurassic and Cretaceous age are conspicuous by their absence in the Changdu area of the Qiangtang Terrane. By contrast, in the Basu-Chayu area of the Lhasa Terrane, there was a change from shallow marine sediments in the Middle Jurassic to volcano-sedimentary successions in the Late Cretaceous (Table S1). This indicates that, whereas the Changdu area was located along a passive continental margin, the Basu-Chayu area was located on an active continental margin, and the Bangong-Nujiang Meso-Tethyan Oceanic crust only underwent southward subduction beneath the Lhasa Terrane from the Middle Jurassic to Early Cretaceous.

Paleomagnetic studies indicate that the Lhasa Terrane reached a similar paleolatitude to the Qiangtang Terrane at around 135 Ma (Song et al., 2017; Figure 2a), suggesting strongly that the initial collision of the two terranes probably occurred at ~135 Ma. Magmatism in the Basu-Chayu and Tengchong-Lianghe areas, however, was most intense between ~135 and 110 Ma (Figure 1b; Chiu et al., 2009; Xu et al., 2012; Xie et al., 2016). This is similar to the case for the Lhasa and Qiangtang terranes along the BNSZ in central Tibet. The occurrence of magmatism along the BNSZ almost 25 Ma after the initial collision has been explained by soft collision, which was triggered by the slab roll-back and break-off of the southward subducting Bangong-Nujiang Oceanic slab and associated shortening of the upper crust (Zhu et al., 2011b; Zhu et al., 2016).

4.3 Late Cretaceous transtension in the Eastern Tibetan Plateau

As mentioned in the description of the regional geology, large volumes of Late Cretaceous (105~75 Ma) granite were emplaced along the north-south strike (DXGF) of the Yidun Arc (Wang et al., 2014a; Wang et al., 2014b). In addition, a slow Cretaceous regional cooling and uplift (20–45 m/Myr) is recorded by the zircon (U-Th)/He (ZHe) and apatite fission track (AFT) ages of the pre-Cretaceous igneous and sedimentary rocks of the Eastern Tibetan Plateau (Figures 1b and 2b; e.g., Lai et al., 2007; Wilson & Fowler, 2011; Tian et al., 2014; Zhao et al., 2017; Leng et al., 2018). This regional uplift event is also reflected by a reduction in the proportion of red beds during the Cretaceous (Figure 1b and Table S1). Recently, Liu-Zeng et al. (2018) reported a moderate to high exhumation rate (70–300 m/Myr) for the mid- to late-Cretaceous (120–80Ma) in the Deqin-Weixi area of the eastern part of the Qiangtang Terrene (Figure 1b).

These regional events indicate that the Eastern Tibetan Plateau was controlled by the same geodynamic regime during the Late Cretaceous. However, the nature of the geodynamic regime is vigorously debated and still poorly constrained, despite its importance in marking a change from collision (Lhasa-Qiangtang) to assembly (Indo-Asian). Three models have been proposed to explain the Late Cretaceous tectonic events in the Eastern Tibetan Plateau: (1) post-orogenic extension after the collision of the Yidun Arc with the Songpan-Ganzi Terrane (Hou et al., 2003); (2) northward subduction of the Neo-Tethyan Oceanic slab (Reid et al., 2007); (3) intra-plate extension in a post-collisional environment related to the Lhasa-Qiangtang collision (Wang et al., 2014a; Wang et al., 2014b; Yang et al., 2016).

Several occurrences of intra-plate igneous rocks and evidence of regional uplift in the Yidun Arc and Songpan-Ganzi Terrane during the Early Jurassic suggest strongly that the post-orogenic extension of the two terranes took place during the Jurassic (Wang et al., 2014b). The driver of Late Cretaceous extension is more poorly understood. Subduction of the Neo-Tethyan Oceanic slab cannot explain why igneous activity in the Eastern Tibetan Plateau was intense during the Late Cretaceous but occurred rarely during the Jurassic and Early Cretaceous. This is because numerous studies have shown that the Neo-Tethyan Oceanic slab subducted northward beneath the Lhasa Terrane from ~190 Ma until ~60 Ma (Chu et al., 2006; Chiu et al., 2009; Zhang et al., 2012). The occurrence of Late Cretaceous magmatism in the Eastern Tibetan Plateau indicates that the geodynamic setting of this region changed suddenly at the end of the Early Cretaceous. The model of intra-plate extension in a post-collisional environment related to the Lhasa-Qiangtang collision proposed by Wang et al. (2014a & 2014b) also fails to explain this rapid change in the regional geodynamic regime. In addition, none of the models referred to above discussed the petrogenesis of the Late Cretaceous intrusions in the eastern Qiangtang Terrane (Changdu area), even though this would have provided important insights into the Late Cretaceous tectonic evolution of the Eastern Tibetan Plateau.

The fact that the Ruduo syenite and Bangda A-type granite intrusions were emplaced in the eastern Qiangtang terrane along the LSSZ at ~ 76 Ma provides clear evidence of an intra-plate extensional tectonic setting at this time. Furthermore, ages of 87.8 ~83.8 Ma from inherited zircon crystals in the Ruduo syenite indicate that the onset of magmatism in the area was earlier and thus the change to an extensional environment also occurred earlier, probably at ~87.8 Ma. Contemporaneously, with the emplacement of the Ruduo syenite and the Bangda granite and other intrusions along the LSSZ, large volumes of intra-plate 105~75 Ma A-type and adakite-like intrusions were emplaced along the north-south strike (DXGF) of the Yidun Arc. As mentioned above, the Yidun Arc was associated with a wide Triassic back-arc basin and bimodal volcanism (which was controlled by NS or NNW strike-slip faults). This indicates that the Yidun Arc experienced strong extension during the Triassic. These zones of weakness (e.g., Paleo-Tethyan Ocean Suture zones) are favorable for the development of late faults and could be established from the ages of syn-tectonic metamorphic or igneous rocks (Tian et al., 2014). The fact that two Late Cretaceous igneous belts developed along strike-slip faults is evidence of intense relative motion between two different pairs of terranes in the Eastern Tibetan Plateau and supports the idea that there was a transtension between the Lhasa and Qiangtang Terranes during the Late Cretaceous.

Given that large volumes of igneous rocks were emplaced in the Basu-Chayu and West Yunnan Area between 130 Ma and 110 Ma, as a result of the Bangong-Nujiang Oceanic slab roll-back and break-off (Xie et al., 2016; Zhu et al., 2016), we infer that this event probably marked an important change in the regional geodynamic regime of the Eastern Tibetan Plateau. Before the slab break-off, there was a cushion between the Lhasa and Qiangtang Terranes, which was able to absorb the pressure from the northward-moving Lhasa Terrane through upper crustal shortening, allowing for a soft Early Cretaceous collision (Zhu et al., 2016). The subduction of the Neo-Tethys oceanic crust probably drove the Lhasa Terrane northward during Cretaceous, which is reflected by the northward motion of the Tibetan Himalayan and Indian plates (Lippert et al., 2014; Song et al., 2017; Figure 2a). After the Bangong-Nujiang Tethyan slab break-off, however, this cushion was lost. Thus, in order to absorb the pressure from the Lhasa Terrane, the other terranes in the Eastern Tibetan Plateau moved relative to each other. Just as the Indo-Asian collision triggered reactivation of the Paleo-Tethyan Suture zone, so intra-plate transtension dominated the Eastern Tibetan Plateau between 105~74 Ma and in the process reactivated the LSSZ and DXGF (Figure 9).

5 Conclusions

(1) The Bangda A-type granite and Ruduo syenite were emplaced along the Longmu-Shuanghu Suture zone at ~78 Ma and ~74 Ma, respectively.

(2) The Bangda magma originated through partial melting of a high-K basaltic layer in the lower crust. The Ruduo syenite magma formed by partial melting of the same layer but owes its composition to the fact that the layer was more mafic than below the Bangda intrusion and was altered by H_2O and CO_2. The composition of the magma was also affected by a minor contribution of mantle derived melt.

(3) A postcollisional Late Cretaceous transtensional tectonic model is proposed for the Lhasa-Qiangtang collision in the Eastern Tibetan Plateau, based on the evidence of this study for alkaline magmatism along the LSSZ at between ~78 and 74 Ma and A-type and adakite-like intrusions along the axis of the Yidun Arc between 105~75 Ma.

Acknowledgments

This study was supported by the strategic priority research program (B) of the Chinese Academy of Sciences (XDB18030000), the national Key R&D Program of China (2016YFC0600503), and the National Natural Science Foundation of China (41603052). We would like to thank Dr. Ke-Qiang Peng and Dr. Jin-Xiang Li for their assistance with the field work, Prof. Zhao-Chu Hu and Liang Li for conducting the LA-(MC)-ICP-MS zircon U-Pb and Hf isotope analyses, Prof. Ke-Qing Zong for the whole-rock Sr, Nd and Pb isotope analyses, Prof. Qiu-Li Li, Dr. Shun-Hu

Yang, Mr. Guo-Qiang Tang, and Ms. Hong-Xia Ma for the SIMS zircon O isotope analyses, and Ms. Jing Hu for the major and trace elements analyses. We are grateful for the constructive reviews of Kwan-Nang Pang and the anonymous reviewer that improved this manuscript, and the editorial assistance of Editor Stephen Parman and Fang-Zhen Teng. The data presented are included in the supporting information file and deposited in the repository of Figshare https://figshare.com/articles/Supporting_information_docx/7895495.

References

Blichert-Toft, J., & Albarède, F. (1997). The Lu-Hf isotope geochemistry of chondrites and the evolution of the mantle-crust system. *Earth and Planetary Science Letters*, *148*(1), 243-258. https://doi.org/10.1016/S0012-821X(97)00040-X

Bonin, B. (2007). A-type granites and related rocks: Evolution of a concept, problems and prospects. *Lithos*, *97*(1-2), 1-29. https://doi.org/10.1016/j.lithos.2006.12.007

Chiu, H. Y., Chung, S. L., Wu, F. Y., Liu, D. Y., Liang, Y. H., Lin, I. J. et al. (2009). Zircon U-Pb and Hf isotopic constraints from eastern Transhimalayan batholiths on the precollisional magmatic and tectonic evolution in southern Tibet. *Tectonophysics*, *477*(1-2), 3-19. https://doi.org/10.1016/j.tecto.2009.02.034

Chu, M. F., Chung, S. L., Song, B. A., Liu, D. Y., O'Reilly, S. Y., Pearson, N. J. et al. (2006). Zircon U-Pb and Hf isotope constraints on the Mesozoic tectonics and crustal evolution of southern Tibet. *Geology*, *34*(9), 745-748. https://doi.org/10.1130/022725.1

Chung, S. L., Chu, M. F., Zhang, Y. Q., Xie, Y. W., Lo, C. H., Lee, T. Y. et al. (2005). Tibetan tectonic evolution inferred from spatial and temporal variations in post-collisional magmatism. *Earth-Science Reviews*, *68*(3-4), 173-196. https://doi.org/10.1016/j.earscirev.2004.05.001

Condamine, P., & Médard, E. (2014). Experimental melting of phlogopite-bearing mantle at 1 GPa: Implications for potassic magmatism. *Earth and Planetary Science Letters, 397*, 80-92. https://doi.org/10.1016/j.epsl.2014.04.027

Dai, F. Q., Zhao, Z. F., & Zheng, Y. F. (2017). Partial melting of the orogenic lower crust: Geochemical insights from post-collisional alkaline volcanics in the Dabie orogen. *Chemical Geology*, *454*, 25-43. https://doi.org/10.1016/j.chemgeo.2017.02.022

Dai, J., Wang, C., Hourigan, J., & Santosh, M. (2013). Insights into the early Tibetan Plateau from (U–Th)/He thermochronology. *Journal of the Geological Society*, *170*(6), 917-927. https://doi.org/10.1144/jgs2012-076

Dall'Agnol, R., & Oliveira, de D. C. (2007). Oxidized, magnetite-series, rapakivi-type granites of Carajás, Brazil: implications for classification and petrogenesis of A-type granites. *Lithos*, *93*(3-4), 215-233. https://doi.org/10.1016/j.lithos.2006.03.065

Eby, G. N., Woolley, A. R., Din, V., & Platt, G. (1998). Geochemistry and petrogenesis of nepheline syenites: Kasungu-Chipala, Ilomba, and Ulindi nepheline syenite intrusions, North Nyasa Alkaline Province, Malawi. *Journal of Petrology*, *39*(8), 1405-1424. https://doi.org/10.1093/petrology/39.8.1405

Fan, W., Wang, Y., Zhang, A., Zhang, F., & Zhang, Y. (2010). Permian arc–back-arc basin development along the Ailaoshan tectonic zone: Geochemical, isotopic and geochronological evidence from the Mojiang volcanic rocks, Southwest China. *Lithos*, *119*(3), 553-568. https://doi.org/10.1016/j.lithos.2010.08.010

Frost, C. D., & Frost, B. R. (2011). On Ferroan (A-type) Granitoids: their Compositional Variability and Modes of Origin. *Journal of Petrology*, *52*(1), 39-53. https://doi.org/10.1093/petrology/egq070

Griffin, W. L., Pearson, N. J., Belousova, E., Jackson, S. E., van Achterbergh, E., O'Reilly, S. Y. et al. (2000). The Hf isotope composition of cratonic mantle: LAM-MC-ICPMS analysis of zircon megacrysts in kimberlites. *Geochimica Et Cosmochimica Acta*, *64*(1), 133-147. https://doi.org/10.1016/s0016-7037(99)00343-9

Griffin, W. L., Wang, X., Jackson, S. E., Pearson, N. J., O'Reilly, S. Y., Xu, X. et al. (2002). Zircon chemistry and magma mixing, SE China: In-situ analysis of Hf isotopes, Tonglu and Pingtan igneous complexes. *Lithos*, *61*(3–4), 237-269. https://doi.org/10.1016/S0024-4937(02)00082-8

Harris, N. B. W., Xu, R. H., Lewis, C. L., Hawkesworth, C. J., & Zhang, Y. Q. (1988). Isotope geochemistry of the 1985 tibet geotraverse, lhasa to golmud. *Philosophical Transactions of the Royal Society a-Mathematical Physical and Engineering Sciences*, *327*(1594), 263-285. https://doi.org/10.1098/rsta.1988.0129

Hou, Z. Q., Yang, Y. Q., Wang, H. P., Qu, X. M., Lv, Q. T., Huang, D. H. et al. (2003). Collision-Orogenic Progress and Mineralization System of Yidun Arc. *Geological Publishing House, Beijing (335 pp., in Chinese)*.

Huppert, H. E., & Sparks, R. S. J. (1988). The generation of granitic magmas by intrusion of basalt into continental crust. *Journal of Petrology, 29*(3), 599-624. https://doi.org/10.1093/petrology/29.3.599

Jackson, W. T., Robinson, D. M., Weislogel, A. L., Shang, F., & Jian, X. (2018). Mesozoic Development of Nonmarine Basins in the Northern Yidun Terrane: Deposition and Deformation in the Eastern Tibetan Plateau Prior to the India-Asia Collision. *Tectonics*, *37*(8), 2466-2485. https://doi.org/10.1029/2018tc004995

Kapp, P., DeCelles, P. G., Gehrels, G. E., Heizier, M., & Ding, L. (2007). Geological records of the Lhasa-Qiangtang and Indo-Asian collisions in the Nima area of central Tibet. *Geological Society of America Bulletin*, *119*(7-8), 917-932. https://doi.org/10.1130/b26033.1

Kapp, P., Murphy, M. A., Yin, A., Harrison, T. M., Ding, L., & Guo, J. H. (2003). Mesozoic and Cenozoic tectonic evolution of the Shiquanhe area of western Tibet. *Tectonics*, *22*(4). https://doi.org/10.1029/2001tc001332

Kapp, P., Yin, A., Harrison, T. M., and Ding, L. (2005). Cretaceous-Tertiary shortening, basin development, and volcanism in central Tibet. *Geological Society of America Bulletin*, *117*(7-8), 865-878. https://doi.org/10.1130/1325595.1

Kaszuba, J. P., & Wendlandt, R. F. (2000). Effect of Carbon Dioxide on Dehydration Melting Reactions and Melt Compositions in the Lower Crust and the Origin of Alkaline Rocks. *Journal of Petrology*, *41*(3), 363-386. https://doi.org/10.1093/petrology/41.3.363

Keto, L. S., & Jacobsen, S. B. (1987). Nd and Sr isotopic variations of Early Paleozoic oceans. *Earth and Planetary Science Letters*, *84*(1), 27-41. https://doi.org/10.1016/0012-821X(87)90173-7

Lai, Q. Z., Ding, L., Wang, H. W., Yue, Y. H., & Cai, F. L. (2007). Constraining the stepwise migration of the eastern Tibetan Plateau margin by apatite fission track thermochronology. *Science in China Series D-Earth Sciences*, *50*(2), 172-183. https://doi.org/10.1007/s11430-007-2048-7

Laporte, D., Lambart, S., Schiano, P., & Ottolini, L. (2014). Experimental derivation of nepheline syenite and phonolite liquids by partial melting of upper mantle peridotites. *Earth and Planetary Science Letters*, *404*, 319-331. https://doi.org/10.1016/j.epsl.2014.08.002

Legendre, C., Maury, R. C., Caroff, M., Guillou, H., Cotten, J., Chauvel, C. et al. (2005). Origin of Exceptionally Abundant Phonolites on Ua Pou Island (Marquesas, French Polynesia): Partial Melting of Basanites Followed by Crustal Contamination. *Journal of Petrology*, *46*(9), 1925-1962. https://doi.org/10.1093/petrology/egi043

Leng, C. B., Cooke, D. R., Hou, Z. Q., Evans, N. J., Zhang, X. C., Chen, W. T. et al. (2018). Quantifying Exhumation at the Giant Pulang Porphyry Cu-Au Deposit Using U-Pb-He Dating. *Economic Geology*, *113*(5), 1077-1092. https://doi.org/10.5382/econgeo.2018.4582

Li, C. F., Chu, Z. Y., Guo, J. H., Li, Y. L., Yang, Y. H., & Li, X. H. (2015). A rapid single column separation scheme for high-precision Sr-Nd-Pb isotopic analysis in geological samples using thermal ionization mass spectrometry. *Analytical Methods*, *7*(11), 4793-4802. https://doi.org/10.1039/c4ay02896a

Li, X. H., Li, Z. X., Li, W. X., Wang, X. C., & Gao, Y. (2013). Revisiting the "C-type adakites" of the Lower Yangtze River Belt, central eastern China: In-situ zircon Hf-O isotope and geochemical constraints. *Chemical Geology*, *345*, 1-15. https://doi.org/10.1016/j.chemgeo.2013.02.024

Lippert, P. C., van Hinsbergen, D. J. J., & Dupont-Nivet, G. (2014), Early Cretaceous to present latitude of the central proto-Tibetan Plateau: A paleomagnetic synthesis with implications for Cenozoic tectonics, paleogeography, and climate of Asia, in *Toward an Improved Understanding of Uplift Mechanisms and the Elevation History of the Tibetan Plateau*, edited by J. Nie, B. K. Horton and G. D. Hoke, *Geological Society of America*. https://doi.org/10.1130/2014.2507(01)

Litvinovsky, B. A., Jahn, B. M., & Eyal, M. (2015). Mantle-derived sources of syenites from the A-type igneous suites - New approach to the provenance of alkaline silicic magmas. *Lithos*, *232*, 242-265. https://doi.org/10.1016/j.lithos.2015.06.008

Liu-Zeng, J., Zhang, J., McPhillips, D., Reiners, P., Wang, W., Pik, R. et al. (2018). Multiple episodes of fast exhumation since Cretaceous in southeast Tibet, revealed by low-temperature thermochronology. *Earth and Planetary Science Letters*, *490*, 62-76. https://doi.org/10.1016/j.epsl.2018.03.011

Liu, C., Zhao, G., Liu, F., & Shi, J. (2017). Detrital zircon U-Pb and Hf isotopic and whole-rock geochemical study of the Bayan Obo Group, northern margin of the North China Craton: Implications for Rodinia reconstruction. *Precambrian Research*, *303*, 372-391. https://doi.org/10.1016/j.precamres.2017.04.033

Liu, Y. S., Gao, S., Hu, Z. C., Gao, C. G., Zong, K. Q., & Wang, D. B. (2010). Continental and Oceanic Crust Recycling-induced Melt-Peridotite Interactions in the Trans-North China Orogen: U-Pb Dating, Hf Isotopes and Trace Elements in Zircons from Mantle Xenoliths. *Journal of petrology*, *51*(1-2), 537-571. https://doi.org/10.1093/petrology/egp082

Lu, Y. J., Kerrich, R., McCuaig, T. C., Li, Z. X., Hart, C. J. R., Cawood, P. A. et al. (2013). Geochemical, Sr-Nd-Pb, and Zircon Hf-O Isotopic Compositions of Eocene-Oligocene Shoshonitic and Potassic Adakite-like Felsic

Intrusions in Western Yunnan, SW China: Petrogenesis and Tectonic Implications. *Journal of Petrology, 54*(7), 1309-1348. https://doi.org/10.1093/petrology/egt013

Ludwig, K. R. (2003). ISOPLOT 3.00: A Geochronological Toolkit for Microsoft Excel. *Berkeley: Berkeley Geochronology Center, California*.

Maniar, P. D., & Piccoli, P. M. (1989). Tectonic discrimination of granitoids. *Bulletin of the Geological Society of America*, *101*(5), 635. https://doi.org/10.1130/0016-7606(1989)101<0635:TDOG>2.3.CO;2

Middlemost, E. A. K. (1994). Naming materials in the magma/igneous rock system. *Earth-Science Reviews*, *37*(3–4), 215-224. https://doi.org/10.1016/0012-8252(94)90029-9

Murphy, M. A., Yin, A., Harrison, T. M., Dürr, S. B., Chen, Z., Ryerson, F. J. et al. (1997). Did the Indo-Asian collision alone create the Tibetan plateau? *Geology*, *25*(8), 719-722. https://doi.org/10.1130/0091-7613(1997)025<0719:DTIACA>2.3.CO;2

Patiño Douce, A. E. (1997), Generation of metaluminous A-type granites by low-pressure melting of calc-alkaline granitoids. *Geology, 25*(8), 743-746. https://doi.org/10.1130/0091-7613(1997)025<0743:GOMATG>2.3.CO;2

Peng, T., Zhao, G., Fan, W., Peng, B., & Mao, Y. (2015). Late Triassic granitic magmatism in the Eastern Qiangtang, Eastern Tibetan Plateau: Geochronology, petrogenesis and implications for the tectonic evolution of the Paleo-Tethys. *Gondwana Research*, *27*(4), 1494-1508. https://doi.org/10.1016/j.gr.2014.01.009

Plank, T., & Langmuir, C. H. (1998). The chemical composition of subducting sediment and its consequences for the crust and mantle. *Chemical Geology*, *145*(3-4), 325-394. https://doi.org/10.1016/s0009-2541(97)00150-2

Pullen, A., & Kapp, P. (2014), Mesozoic tectonic history and lithospheric structure of the Qiangtang terrane: Insights from the Qiangtang metamorphic belt, central Tibet, in *Toward an Improved Understanding of Uplift Mechanisms and the Elevation History of the Tibetan Plateau*, edited by J. Nie, B. K. Horton and G. D. Hoke, *Geological Society of America*. https://doi.org/10.1130/2014.2507(04)

Qi, L., Hu, J., & Gregoire, D. C. (2000). Determination of trace elements in granites by inductively coupled plasma mass spectrometry. *Talanta*, *51*(3), 507-513. https://doi.org/10.1016/S0039-9140(99)00318-5

Qian, Q., & Hermann, J. (2013). Partial melting of lower crust at 10–15 kbar: constraints on adakite and TTG formation. *Contributions to Mineralogy and Petrology, 165*(6), 1195-1224. https://doi.org/10.1007/s00410-013-0854-9

Qu, X. M., Hou, Z. Q., & Tang, S. H. (2003). Age of intraplate volcanism in the back-arc area of Yidun island arc and its significance. *Petrologica Et Mineralogica*, *22*(2), 131-137. (in Chinese with English abstract).

Qu, X. M., Hou, Z. Q., & Zhou, S. G. (2002). Geochemical and Nd, Sr isotopic study of the post-orogenic granites in the Yidun arc belt of northern Sanjiang region, southwestern China. *Resource Geology*, *52*(2), 163-172. https://doi.org/10.1111/j.1751-3928.2002.tb00128.x

Rapp, R. P., Watson, E. B., & Miller, C. F. (1991). Partial melting of amphibolite eclogite and the origin of archean trondhjemites and tonalites. *Precambrian Research, 51*(1-4), 1-25. https://doi.org/10.1016/0301-9268(91)90092-o

Rapp, R. P., & Watson, E. B. (1995). Dehydration Melting of Metabasalt at 8–32 kbar: Implications for Continental Growth and Crust-Mantle Recycling. *Journal of Petrology, 36*(4), 891-931. https://doi.org/10.1093/petrology/36.4.891

Reid, A., Wilson, C. J. L., Shun, L., Pearson, N., & Belousova, E. (2007). Mesozoic plutons of the Yidun Arc, SW China: U/Pb geochronology and Hf isotopic signature. *Ore Geology Reviews*, *31*(1-4), 88-106. https://doi.org/10.1016/j.oregeorev.2004.11.003

Rickwood, P. C. (1989). Boundary lines within petrologic diagrams which use oxides of major and minor elements. *Lithos, 22*(4), 247-263. https://doi.org/10.1016/0024-4937(89)90028-5

Rohrmann, A., Kapp, P., Carrapa, B., Reiners, P. W., Guynn, J., Ding, L. et al. (2012). Thermochronologic evidence for plateau formation in central Tibet by 45 Ma. *Geology*, *40*(2), 187-190. https://doi.org/10.1130/g32530.1

Scherer, E., Münker, C., & Mezger, K. (2001). Calibration of the lutetium-hafnium clock. *Science*, *293*(5530), 683-687. https://doi.org/10.1126/science.1061372

Siegel, K., Vasyukova, O. V., & Williams-Jones, A. E. (2018). Magmatic evolution and controls on rare metal-enrichment of the Strange Lake A-type peralkaline granitic pluton, Québec-Labrador. *Lithos*, *308-309*, 34-52. https://doi.org/10.1016/j.lithos.2018.03.003

Sisson, T. W., Ratajeski, K., Hankins, W. B., & Glazner, A. F. (2005). Voluminous granitic magmas from common basaltic sources. *Contributions to Mineralogy and Petrology*, *148*(6), 635-661. https://doi.org/10.1007/s00410-004-0632-9

Song, P. P., Ding, L., Li, Z. Y., Lippert, P. C., & Yue, Y. H. (2017). An early bird from Gondwana: Paleomagnetism of Lower Permian lavas from northern Qiangtang (Tibet) and the geography of the Paleo-Tethys. *Earth and*

Planetary Science Letters, *475*, 119-133. https://doi.org/10.1016/j.epsl.2017.07.023

Stern, R. J. (2002). Subduction zones. *Reviews of Geophysics*, *40*(4). https://doi.org/10.1029/2001rg000108

Sun, S. S., & McDonough, W. F. (1989). Chemical and isotopic systematics of oceanic basalts: implications for mantle composition and processes. *Geological Society, London, Special Publications*, *42*(1), 313-345. https://doi.org/10.1144/GSL.SP.1989.042.01.19

Tanaka, T., Togashi, S., Kamioka, H., Amakawa, H., Kagami, H., Hamamoto, T. et al. (2000). JNdi-1: a neodymium isotopic reference in consistency with LaJolla neodymium. *Chemical Geology*, *168*(3), 279-281. https://doi.org/10.1016/S0009-2541(00)00198-4

Thomsen, T. B., & Schmidt, M. W. (2008). Melting of carbonated pelites at 2.5-5.0 GPa, silicate-carbonatite liquid immiscibility, and potassium-carbon metasomatism of the mantle. *Earth and Planetary Science Letters*, *267*(1-2), 17-31. https://doi.org/10.1016/j.epsl.2007.11.027

Tian, Y. T., Kohn, B. P., Hu, S. B., & Gleadow, A. J. W. (2014). Postorogenic rigid behavior of the eastern Songpan-Ganze terrane: Insights from low-temperature thermochronology and implications for intracontinental deformation in central Asia. *Geochemistry Geophysics Geosystems*, *15*(2), 453-474. https://doi.org/10.1002/2013gc004951

Todt, W., Cliff, R. A., Hanser, A., & Hofmann, A. (1996). Evaluation of a ^{202}Pb–^{205}Pb Double Spike for High-Precision Lead Isotope Analysis. *Earth processes: reading the isotopic code*, *95*, 429-437. https://doi.org/10.1029/GM095p0429

Torsvik, T. H., Van der Voo, R., Preeden, U., Mac Niocaill, C., Steinberger, B., Doubrovine, P. V. et al. (2012). Phanerozoic polar wander, palaeogeography and dynamics. *Earth-Science Reviews, 114*(3), 325-368. https://doi.org/10.1016/j.earscirev.2012.06.007

Valley, J. W., Lackey, J. S., Cavosie, A. J., Clechenko, C. C., Spicuzza, M. J., Basei, M. A. S. et al. (2005). 4.4 billion years of crustal maturation: oxygen isotope ratios of magmatic zircon. *Contributions to Mineralogy and Petrology*, *150*(6), 561-580. https://doi.org/10.1007/s00410-005-0025-8

Volkmer, J. E., Kapp, P., Horton, B. K., Gehrels, G. E., Minervini, J. M., & Ding, L. (2014). Northern Lhasa thrust belt of central Tibet: Evidence of Cretaceous–early Cenozoic shortening within a passive roof thrust system? *Geological Society of America Special Papers*, *507*, 59-70. https://doi.org/10.1130/2014.2507(03)

Wang, B. Q., Wang, W., Chen, W. T., Gao, J. F., Zhao, X. F., Yan, D. P. et al. (2013a). Constraints of detrital zircon U–Pb ages and Hf isotopes on the provenance of the Triassic Yidun Group and tectonic evolution of the Yidun Terrane, Eastern Tibet. *Sedimentary Geology*, *289*(0), 74-98. https://doi.org/10.1016/j.sedgeo.2013.02.005

Wang, B. Q., Zhou, M. F., Chen, W. T., Gao, J. F., and Yan, D. P. (2013b). Petrogenesis and tectonic implications of the Triassic volcanic rocks in the northern Yidun Terrane, Eastern Tibet. *Lithos*, *175-176*, 285-301. https://doi.org/10.1016/j.lithos.2013.05.013

Wang, X. S., Bi, X. W., Leng, C. B., Zhong, H., Tang, H. F., Chen, Y. W. et al. (2014a). Geochronology and geochemistry of Late Cretaceous igneous intrusions and Mo-Cu-(W) mineralization in the southern Yidun Arc, SW China: Implications for metallogenesis and geodynamic setting. *Ore Geology Reviews*, *61*, 73-95. https://doi.org/10.1016/j.oregeorev.2014.01.006

Wang, X. S., Hu, R. Z., Bi, X. W., Leng, C. B., Pan, L. C., Zhu, J. J. et al. (2014b). Petrogenesis of Late Cretaceous I-type granites in the southern Yidun Terrane: New constraints on the Late Mesozoic tectonic evolution of the eastern Tibetan Plateau. *Lithos*, *208–209*(0), 202-219. https://doi.org/10.1016/j.lithos.2014.08.016

Whalen, J. B., Currie, K. L., & Chappell, B. W. (1987). A-type granites: geochemical characteristics, discrimination and petrogenesis. *Contributions to Mineralogy and Petrology*, *95*(4), 407-419. https://doi.org/10.1007/BF00402202

Wiedenbeck, M., Alle, P., Corfu, F., Griffin, W. L., Meier, M., Oberli, F. et al. (1995). Three natural zircon standards for U-Th-Pb, Lu-Hf, trace element and REE analyses. *Geostandards Newsletter*, *19*(1), 1-23. https://doi.org/10.1111/j.1751-908X.1995.tb00147.x

Wilson, C. J. L., & Fowler, A. P. (2011). Denudational response to surface uplift in east Tibet: Evidence from apatite fission-track thermochronology. *Geological Society of America Bulletin*, *123*(9-10), 1966-1987. https://doi.org/10.1130/b30331.1

Winther, K. T. (1996). An experimentally based model for the origin of tonalitic and trondhjemitic melts. *Chemical Geology, 127*(1), 43-59. https://doi.org/10.1016/0009-2541(95)00087-9

Wolf, M. B., & Wyllie, P. J. (1994). Dehydration-melting of amphibolite at 10 kbar: the effects of temperature and time. *Contributions to Mineralogy and Petrology, 115*(4), 369-383. https://doi.org/10.1007/bf00320972

Wu, T., Xiao, L., Ma, C. Q., Pirajno, F., Sun, Y. & Zhan, Q. Y. (2014). A mafic intrusion of "arc affinity" in a post-orogenic extensional setting: A case study from Ganluogou gabbro in the northern Yidun Arc Belt, eastern

Tibetan Plateau. *Journal of Asian Earth Sciences*, *94*, 139-156. https://doi.org/10.1016/j.jseaes.2014.08.026

Xie, J.-C., Zhu, D.-C., Dong, G., Zhao, Z.-D., Wang, Q., & Mo, X. (2016). Linking the Tengchong Terrane in SW Yunnan with the Lhasa Terrane in southern Tibet through magmatic correlation. *Gondwana Research*, *39*, 217-229. https://doi.org/10.1016/j.gr.2016.02.007

Xu, Y. G., Yang, Q. J., Lan, J. B., Luo, Z. Y., Huang, X. L., Shi, Y. R. et al. (2012). Temporal-spatial distribution and tectonic implications of the batholiths in the Gaoligong-Tengliang-Yingjiang area, western Yunnan: Constraints from zircon U-Pb ages and Hf isotopes. *Journal of Asian Earth Sciences*, *53*, 151-175. https://doi.org/10.1016/j.jseaes.2011.06.018

Yang, L. Q., Deng, J., Dilek, Y., Meng, J. Y., Gao, X., Santosh, M. et al. (2016). Melt source and evolution of I-type granitoids in the SE Tibetan Plateau: Late Cretaceous magmatism and mineralization driven by collision-induced transtensional tectonics. *Lithos*, *245*, 258-273. https://doi.org/10.1016/j.lithos.2015.10.005

Yang, T. N., Ding, Y., Zhang, H. R., Fan, J. W., Liang, M. J., & Wang, X. H. (2014). Two-phase subduction and subsequent collision defines the Paleotethyan tectonics of the southeastern Tibetan Plateau: Evidence from zircon U-Pb dating, geochemistry, and structural geology of the Sanjiang orogenic belt, southwest China. *Geological Society of America Bulletin*, *126*(11-12), 1654-1682. https://doi.org/10.1130/b30921.1

Yin, A., & Harrison, T. M. (2000). Geologic evolution of the Himalayan-Tibetan orogen. *Annual Review of Earth and Planetary Sciences*, *28*, 211-280. https://doi.org/10.1146/annurev.earth.28.1.211

Zhang, H.-F., Zhang, B.-R., Harris, N., Zhang, L., Chen, Y.-L., Chen, N.-S. et al. (2006). U–Pb zircon SHRIMP ages, geochemical and Sr–Nd–Pb isotopic compositions of intrusive rocks from the Longshan–Tianshui area in the southeast corner of the Qilian orogenic belt, China: Constraints on petrogenesis and tectonic affinity. *Journal of Asian Earth Sciences*, *27*(6), 751-764. https://doi.org/10.1016/j.jseaes.2005.07.008

Zhang, K., & Tang, X. (2009). Eclogites in the interior of the Tibetan Plateau and their geodynamic implications. *Chinese Science Bulletin*, *54*(15), 2556. https://doi.org/10.1007/s11434-009-0407-9

Zhang, K. J., Zhang, Y. X., Tang, X. C., & Xia, B. (2012). Late Mesozoic tectonic evolution and growth of the Tibetan plateau prior to the Indo-Asian collision. *Earth-Science Reviews*, *114*(3-4), 236-249. https://doi.org/10.1016/j.earscirev.2012.06.001

Zhao, Z., Bons, P. D., Stübner, K., Wang, G.-H., & Ehlers, T. A. (2017). Early Cretaceous exhumation of the Qiangtang Terrane during collision with the Lhasa Terrane, Central Tibet. *Terra Nova*, *29*(6), 382-391. https://doi.org/10.1111/ter.12298

Zhu, D. C., Li, S. M., Cawood, P. A., Wang, Q., Zhao, Z. D., Liu, S. A. et al. (2016). Assembly of the Lhasa and Qiangtang terranes in central Tibet by divergent double subduction. *Lithos*, *245*, 7-17. https://doi.org/10.1016/j.lithos.2015.06.023

Zhu, D. C., Zhao, Z. D., Niu, Y. L., Dilek, Y., Hou, Z. Q., & Mo, X. X. (2013). The origin and pre-Cenozoic evolution of the Tibetan Plateau. *Gondwana Research*, *23*(4), 1429-1454. https://doi.org/10.1016/j.gr.2012.02.002

Zhu, D. C., Zhao, Z. D., Niu, Y. L., Dilek, Y., & Mo, X. X. (2011a). Lhasa terrane in southern Tibet came from Australia. *Geology*, *39*(8), 727-730. https://doi.org/10.1130/g31895.1

Zhu, D. C., Zhao, Z. D., Niu, Y. L., Mo, X. X., Chung, S. L., Hou, Z. Q. et al. (2011b). The Lhasa Terrane: Record of a microcontinent and its histories of drift and growth. *Earth and Planetary Science Letters*, *301*(1-2), 241-255. https://doi.org/10.1016/j.epsl.2010.11.005

Figure captions

Figure 1. (a) A regional geological map showing terranes and Mesozoic granitoids of the Tibetan Plateau (Wang et al., 2014b), and simplified geological maps of (b) the Eastern Tibetan Plateau, including the eastern portion of the Lhasa and Qiangtang terranes, the Yidun Arc and the western portion of the Songpan-Ganzi Terrane, (c) the Ruduo region and (d) the Bangda region (modified from a public geological map of the Tibetan Bureau of the Geological Survey). Abbreviations: JSSZ=Jinshajiang Suture Zone; GLSZ=Ganzi-Litang Suture Zone; BNSZ=Bangong-Nujiang Suture Zone; YZSZ= Yarlung-Zangbo Suture Zone; DGXF=Dege-Xiangcheng-Geza Faults; YA=Yidun Arc (or Yidun Arc); SM=Simao Terrane; ZL=Zhalong intrusion; GG=Gaogong intrusion; QS=Queershan intrusion; LL=Lianlong intrusion; CML=Cuomolong intrusion; RLL=Ruoluolong intrusion; RYC=Rongyicuo intrusion; GN=Genie; HGL=Hagela (or Haizi); ZJD=Zhujiding intrusion; YGN=Yigongnuo intrusion; HS=Hongshan intrusion; TCG=Tongchanggou intrusion. The geochronological data are from Qu et al. (2002), Lai et al. (2007), Chiu et al. (2009), Wang et al. (2014b), and Liu-Zeng et al. (2018).

Wang, X.-S., Williams-Jones, A.E., Bi, X.-W., Hu, R.-Z., Xiao, J.-F., & Huang, M.-L. (2019).
J. Geophys. Res., Solid Earth 124, 6409–6427.

Figure 2. (a) A paleolatitude versus time plot showing paleomagnetic data for the northern Qiangtang, Lhasa, and Tethyan Himalaya blocks of the Tibetan Plateau. The Eurasian and Gondwanan-Indian paleolatitudes are from Torsvik et al. (2012) and were calculated to the reference location: 34.1° N, 92.4° E. The paleolatitude lines of the Northern Qiangtang, Lhasa, and Tibetan Himalaya Terranes are from Song et al. (2017) and the reference location is 34.1° N and 92.4° E. The timing of the Meso- and Neo-Tethys subduction and the Lhasa-Qiangtang and Indo-Asian terrane collisions (the color bar on the top of the diagram) are based on the motions of the terranes and refer to the review of (Zhu et al., 2013). (b) Thermochronological data for intrusions and sedimentary rocks from the Central and Eastern Tibetan Plateau. Abbreviations: LQ collision = Lhasa-Qiangtang collision; I-A C = Indo-Asia collision; AFT ages = apatite fission-track ages; AHe ages = apatite (U-Th)/He ages; ZHe ages = zircon (U-Th)/He ages. The thermochronological data are from Lai et al. (2007), Wilson and Fowler (2011), Dai et al. (2013), Rohrmann et al. (2012), Tian et al. (2014), Zhao et al. (2017), and Liu-Zeng et al. (2018).

Figure 3. Outcrop photographs and photomicrographs of the Ruduo and Bangda intrusions. (a) an outcrop of the Bangda granite; (b) and (c) cross-polarized light images of the Bangda granite; (d) and (e) outcrops of the Ruduo syenite; (f) and (h) cross-polarized light images of the Ruduo syenite; (g) backscattered electron images of the Ruduo syenite. Abbreviations of minerals: Kf – K-feldspar, Pl – plagioclase, Ab – plagioclase, Bi – biotite, Qtz – quartz, Ap – apatite, Moz – Monazite, Mus – Muscovite, Ca – Carbonate [$Ca_{0.5}(Mg,Fe,Mn)_{0.5}CO_3$], and Zr – Zircon.

Figure 4. Zircon U-Pb concordia diagrams for (a) and (b) sample RD15-01 from the Ruduo syenite, and (d) sample BD15-07 from the Bangda granite. The petrography and locations of the samples are presented in Table S5. (c) cathodoluminescence (CL) images of representative inherited and captured zircon crystals analyzed in situ for their O and U-Pb isotopes. The small ellipses indicate the spots for SIMS analysis of O isotopes, and the large circles the spots for LA-ICPMS analysis of U-Pb isotopes. The numbers in the circles refer to the analysis number. The U-Pb ages and O isotope ratios corresponding to the analysis numbers are reported below the CL images.

Figure 5. (a) A total alkali versus SiO_2 classification diagram showing the compositions of the Bangda and Ruduo intrusions (Middlemost, 1994); (b) A total alkali versus 10000 Ga/Al diagram confirming the classification of both intrusions as A-type (Whalen et al., 1987); (c) A $FeO^T/(FeO^T+MgO)$ versus SiO_2 diagram illustrating the magnesian nature of the Bangda and Ruduo intrusions (Frost & Frost, 2011); (d) A $Al_2O_3/(Na_2O + K_2O)$ versus $Al_2O_3/(CaO+Na_2O+K_2O)$ diagram illustrating the alkaline and metaluminous nature of the Ruduo intrusion and the peraluminous nature of the Bangda intrusion; (e) a plot of K_2O versus SiO_2 showing that the Ruduo intrusion is shoshonitic and the Bangda intrusion is transitional between high K calc-alkaline and shoshonitic (Rickwood, 1989); and (f) a plot of K_2O versus Na_2O classifying both the Ruduo and Bangda intrusions as shoshonitic. The fields of metaluminous, peraluminous, and peralkaline in (d) were taken from Maniar and Piccoli (1989), and the dashed line separating calc-alkaline from alkaline rocks was taken from Whalen et al. (1987).

Figure 6. (a) Chondrite-normalized rare earth element (REE); and (b) primitive mantle-normalized trace element diagrams for the Ruduo and Bangda intrusions. The chondrite and primitive mantle values are from Sun and McDonough (1989).

Figure 7. (a) A $\delta^{18}O$ versus $\varepsilon_{Hf}(t)$ diagram; (b) An age-$\varepsilon_{Hf}(t)$ diagram; (c) A $\varepsilon_{Nd}(t)$ and $(^{87}Sr/^{86}Sr)_i$ diagram; and (d) A $(^{207}Pb/^{204}Pb)t$ versus $(^{206}Pb/^{204}Pb)t$ diagram showing the composition of the Bangda and Ruduo intrusions. The mantle field is from Valley et al. (2005). The data for the Dongdashan S-type granites in the Southern Qiangtang Terrane, Eastern Tibetan Plateau are from Peng et al. (2015). The field of Bangong MORB is from Bao et al. (2007), that of subducting sediments globally is from Plank and Langmuir (1998), the data for the Amdo orthogneiss are from Harris et al. (1988) and the data for the Dongdashan S-type granites are from Peng et al. (2015). The fields of PM (primitive mantle), EM-2, global pelagic sediments, Pacific MORB, and Tethyan basalts are from Fan et al. (2010).

Figure 8. Chemical variation diagrams for the Ruduo and Bangda intrusions. The data for the partial melting experiment starting material and resulting glasses are from Kaszuba and Wendlandt (2000), Sisson et al. (2005), Thomsen and Schmidt (2008) and Laporte et al. (2014).

Figure 9. A model for Late Cretaceous transtension in the Eastern Tibetan Plateau. Not to scale. For an explanation of this model see sections 4.2 and 4.3. Abbreviations: LS = Lhasa Terrane; WQT = Western Qiangtang Terrane; EST = Eastern Qiangtang Terrane; YA = Yidun Arc; SG = Songpan-Ganzi Terrane.

Wang, X.-S., Williams-Jones, A.E., Bi, X.-W., Hu, R.-Z., Xiao, J.-F., & Huang, M.-L. (2019).
J. Geophys. Res., Solid Earth 124, 6409–6427.

Figure 1.

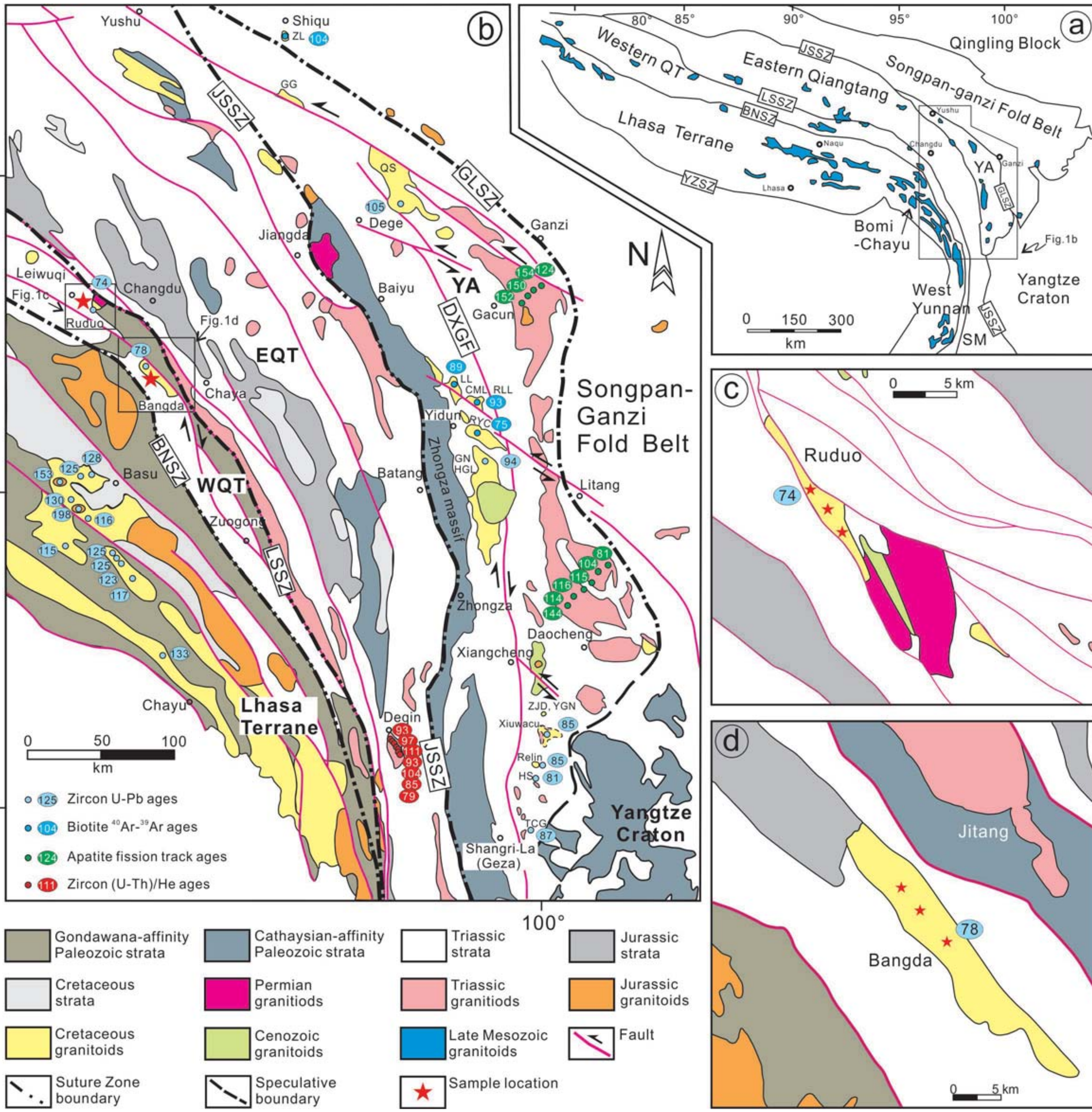

Wang, X.-S., Williams-Jones, A.E., Bi, X.-W., Hu, R.-Z., Xiao, J.-F., & Huang, M.-L. (2019).
J. Geophys. Res., Solid Earth 124, 6409–6427.

Figure 2.

Wang, X.-S., Williams-Jones, A.E., Bi, X.-W., Hu, R.-Z., Xiao, J.-F., & Huang, M.-L. (2019).
J. Geophys. Res., Solid Earth 124, 6409–6427.

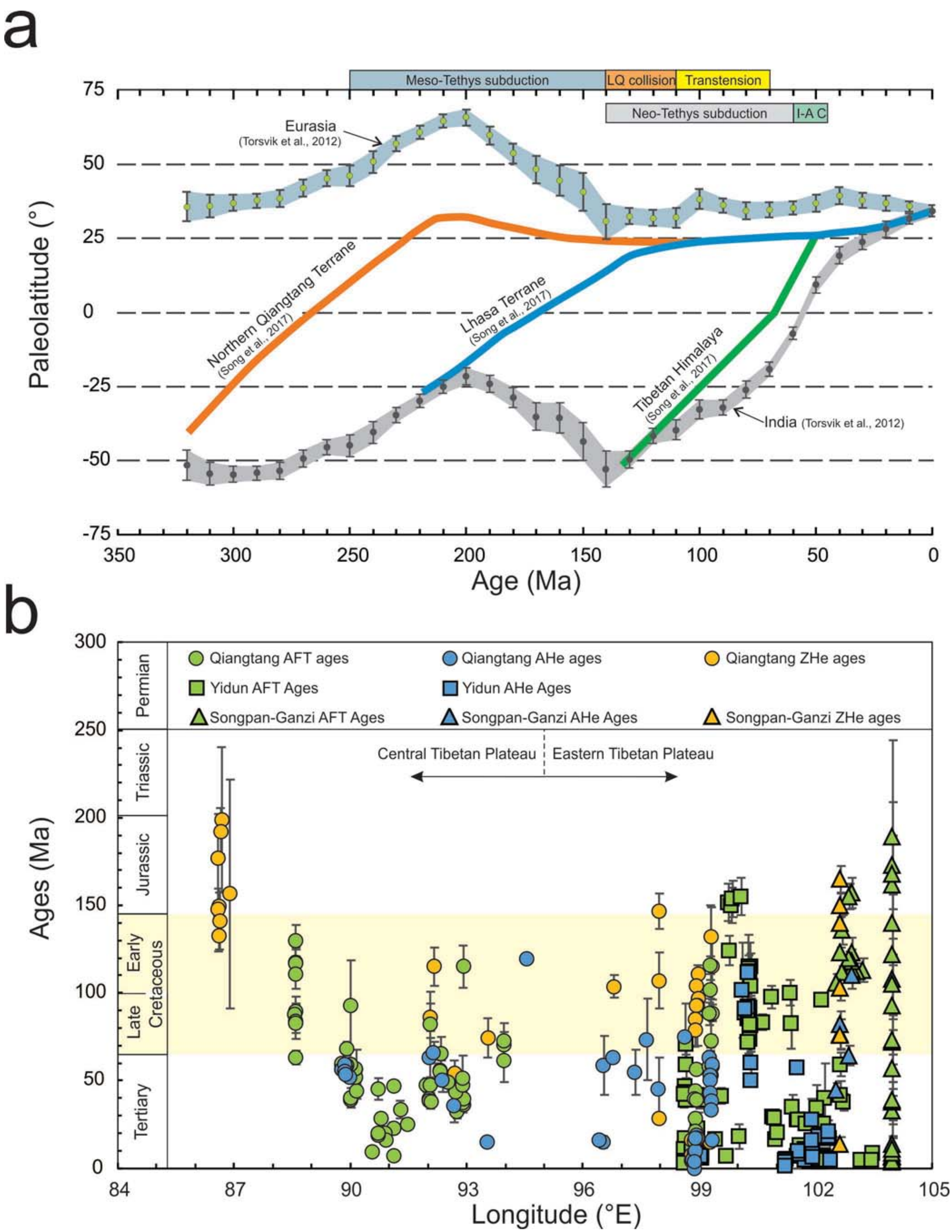

a
Meso-Tethys subduction
LQ collision
Transtension
Neo-Tethys subduction
I-A C
Eurasia
(Torsvik et al., 2012)
Northern Qiangtang Terrane
(Song et al., 2017)
Lhasa Terrane
(Song et al., 2017)
Tibetan Himalaya
(Song et al., 2017)
India (Torsvik et al., 2012)
Paleolatitude (°)
Age (Ma)
b
Qiangtang AFT ages
Qiangtang AHe ages
Qiangtang ZHe ages
Yidun AFT Ages
Yidun AHe Ages
Songpan-Ganzi AFT Ages
Songpan-Ganzi AHe Ages
Songpan-Ganzi ZHe ages
Central Tibetan Plateau
Eastern Tibetan Plateau
Permian
Triassic
Jurassic
Early Cretaceous
Late
Tertiary
Ages (Ma)
Longitude (°E)

Figure 3.

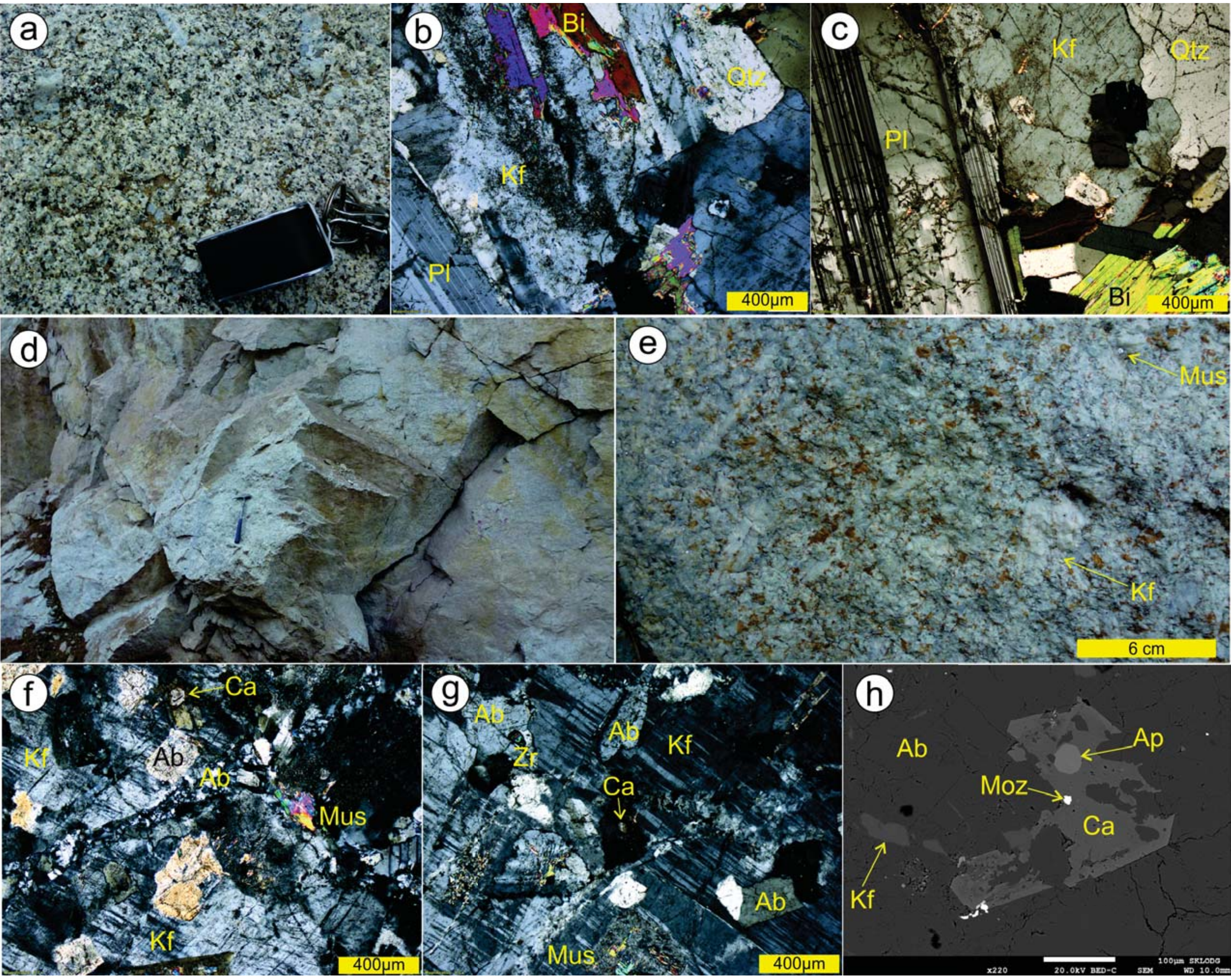
a
b
Bi
Qtz
Kf
Pl
400μm
c
Kf
Qtz
Pl
Bi
400μm
d
e
Mus
Kf
6 cm
f
Ca
Kf
Ab
Ab
Mus
Kf
400μm
g
Ab
Ab
Kf
Zr
Ca
Ab
Mus
400μm
h
Ab
Ap
Moz
Ca
Kf

Figure 4.

Wang, X.-S., Williams-Jones, A.E., Bi, X.-W., Hu, R.-Z., Xiao, J.-F., & Huang, M.-L. (2019).
J. Geophys. Res., Solid Earth 124, 6409–6427.

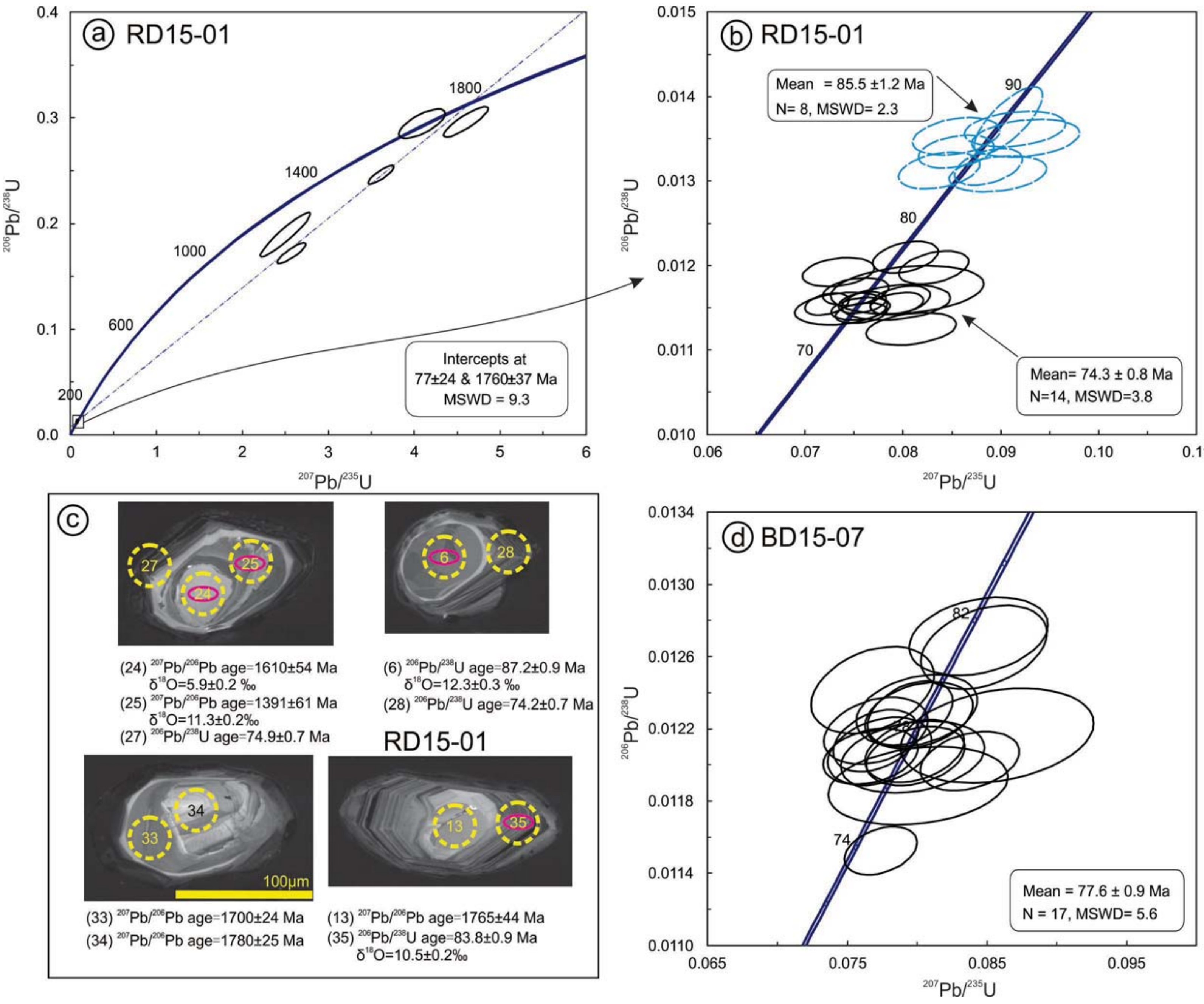

Wang, X.-S., Williams-Jones, A.E., Bi, X.-W., Hu, R.-Z., Xiao, J.-F., & Huang, M.-L. (2019).
J. Geophys. Res., Solid Earth 124, 6409–6427.

Figure 5.

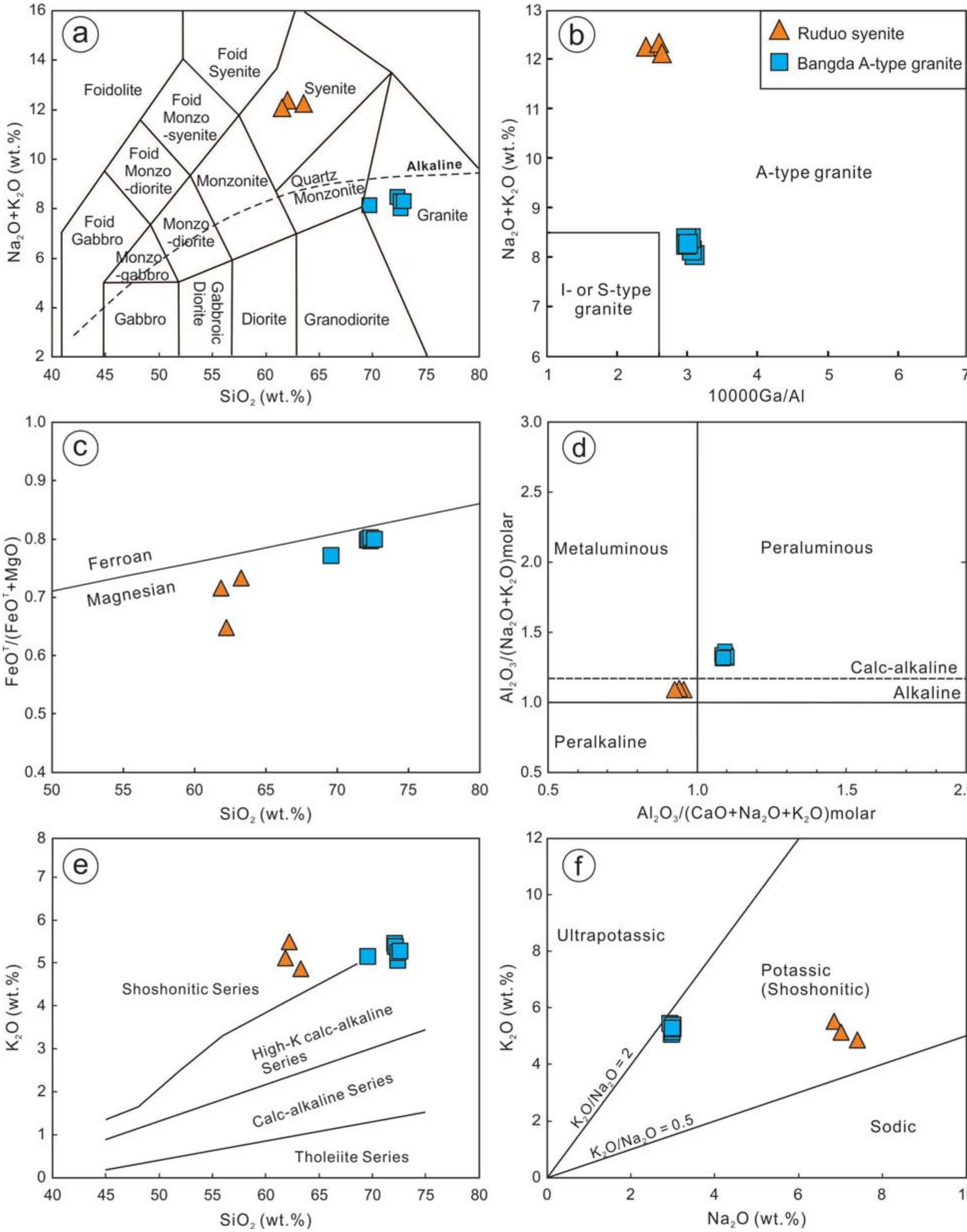

a
Foidolite
Foid Syenite
Foid Monzo -syenite
Syenite
Foid Monzo -diorite
Monzonite
Quartz Monzonite
Alkaline
Foid Gabbro
Monzo -diorite
Monzo -gabbro
Granite
Gabbro
Gabbroic Diorite
Diorite
Granodiorite
Na_2O+K_2O (wt.%)
SiO_2 (wt.%)
b
Ruduo syenite
Bangda A-type granite
A-type granite
I- or S-type granite
10000Ga/Al
c
Ferroan
Magnesian
$FeO^T/(FeO^T+MgO)$
d
Metaluminous
Peraluminous
Calc-alkaline
Alkaline
Peralkaline
NK/A
$Al_2O_3/(Na_2O+K_2O)$molar
$Al_2O_3/(CaO+Na_2O+K_2O)$molar
e
Shoshonitic Series
High-K calc-alkaline Series
Calc-alkaline Series
Tholeiite Series
K_2O (wt.%)
f
Ultrapotassic
Potassic (Shoshonitic)
Sodic
$K_2O/Na_2O = 2$
$K_2O/Na_2O = 0.5$
Na_2O (wt.%)

Figure 6.

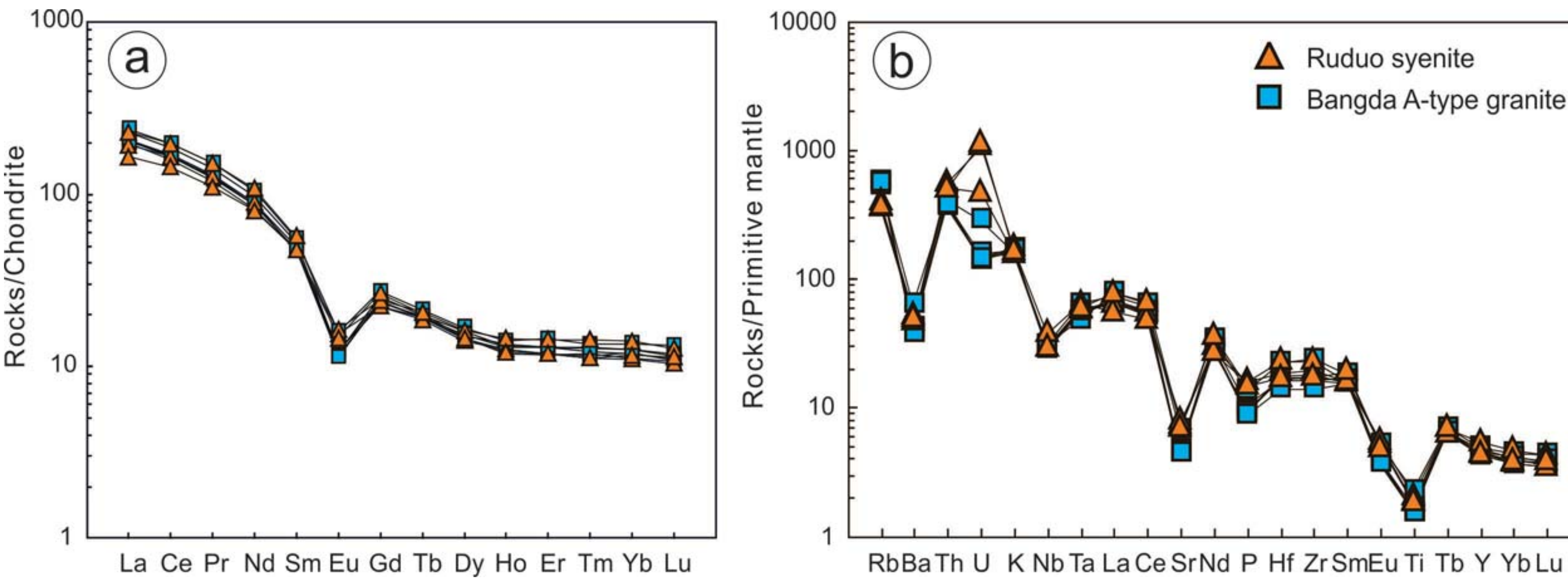
a
1000
100
10
1
Rocks/Chondrite
La Ce Pr Nd Sm Eu Gd Tb Dy Ho Er Tm Yb Lu
b
10000
1000
100
10
1
Rocks/Primitive mantle
Ruduo syenite
Bangda A-type granite
Rb Ba Th U K Nb Ta La Ce Sr Nd P Hf Zr Sm Eu Ti Tb Y Yb Lu

Figure 7.

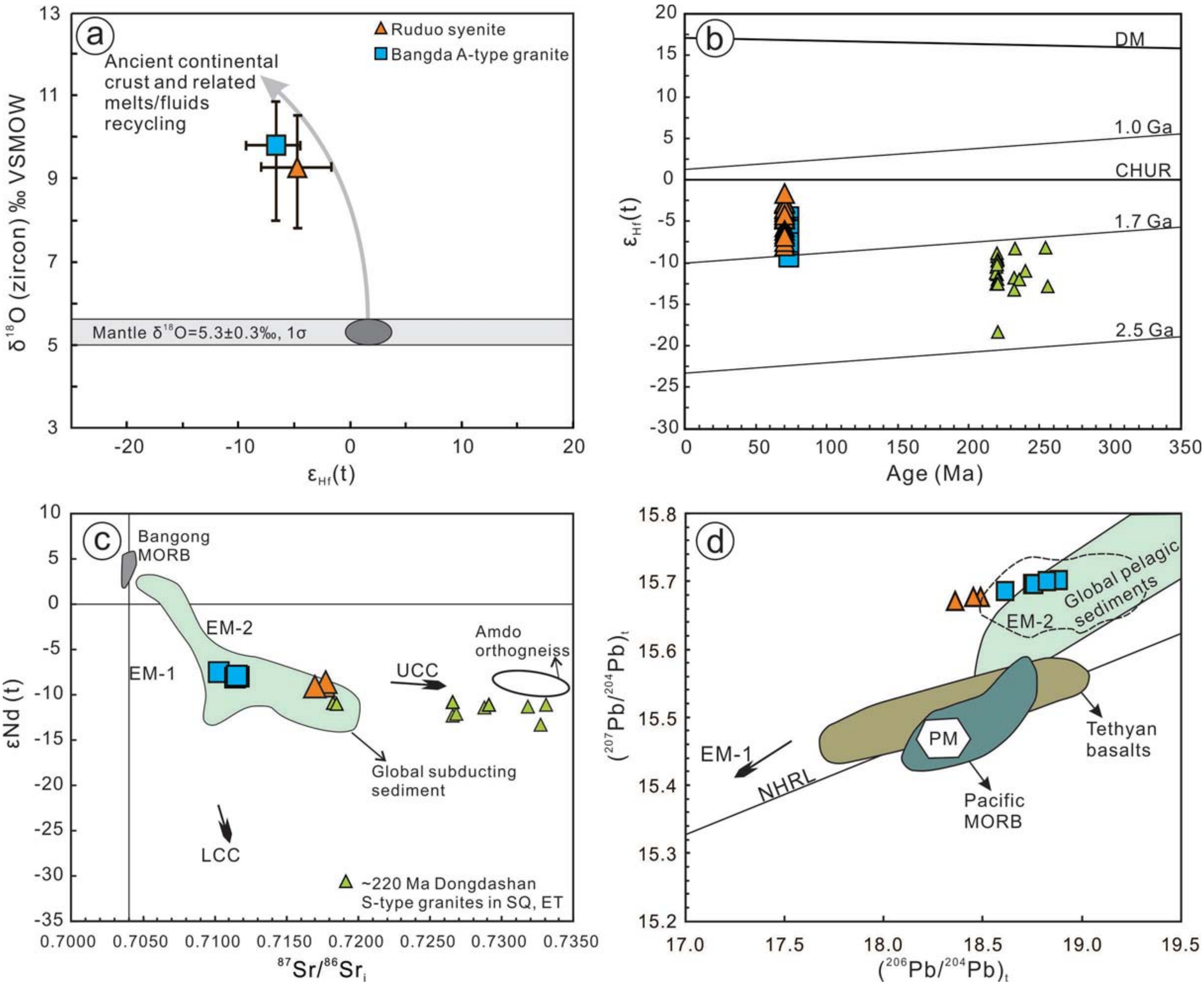

Wang, X.-S., Williams-Jones, A.E., Bi, X.-W., Hu, R.-Z., Xiao, J.-F., & Huang, M.-L. (2019).
J. Geophys. Res., Solid Earth 124, 6409–6427.

Figure 8.

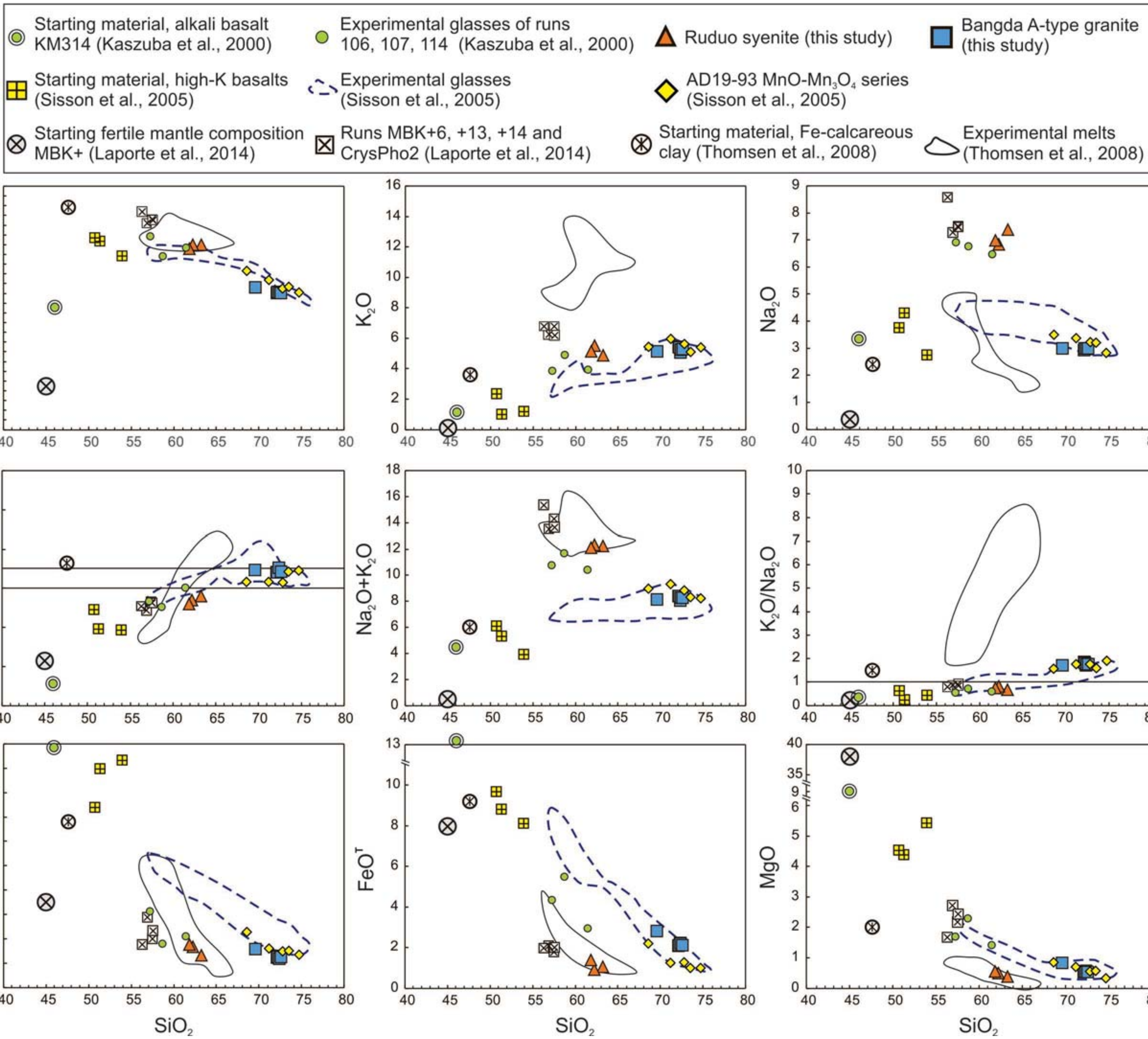

Starting material, alkali basalt KM314 (Kaszuba et al., 2000)
Experimental glasses of runs 106, 107, 114 (Kaszuba et al., 2000)
Ruduo syenite (this study)
Bangda A-type granite (this study)
Starting material, high-K basalts (Sisson et al., 2005)
Experimental glasses (Sisson et al., 2005)
AD19-93 MnO-Mn_3O_4 series (Sisson et al., 2005)
Starting fertile mantle composition MBK+ (Laporte et al., 2014)
Runs MBK+6, +13, +14 and CrysPho2 (Laporte et al., 2014)
Starting material, Fe-calcareous clay (Thomsen et al., 2008)
Experimental melts (Thomsen et al., 2008)
Al_2O_3
K_2O
Na_2O
A/CNK
Na_2O+K_2O
K_2O/Na_2O
CaO
FeO^T
MgO
SiO_2

Figure 9.

Wang, X.-S., Williams-Jones, A.E., Bi, X.-W., Hu, R.-Z., Xiao, J.-F., & Huang, M.-L. (2019).
J. Geophys. Res., Solid Earth 124, 6409–6427.

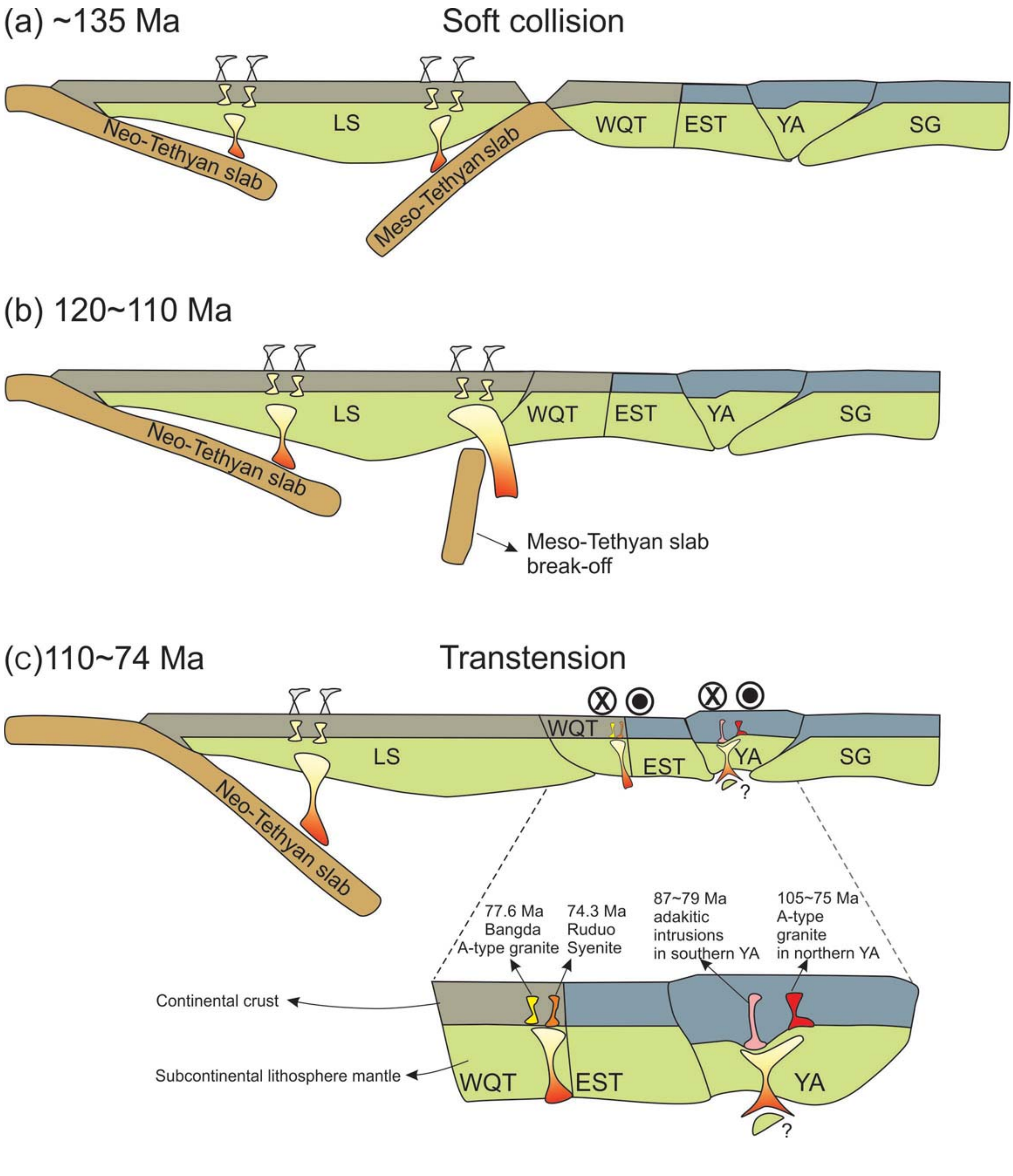

Wang, X.-S., Williams-Jones, A.E., Bi, X.-W., Hu, R.-Z., Xiao, J.-F., & Huang, M.-L. (2019).
J. Geophys. Res., Solid Earth 124, 6409–6427.